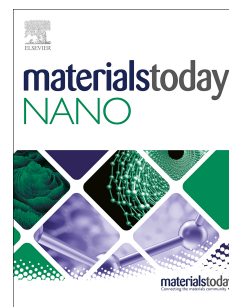


Journal Pre-proof

Defects, Photophysics and Passivation in Pb-Based Colloidal Quantum Dot Photovoltaics

Jiantuo Gan, Miao Yu, Robert L.Z. Hoyer, Kevin P. Musselman, Yan Li, Xiaodong Liu, Yonghao Zheng, Xiaotao Zu, Sean Li, Judith L. MacManus-Driscoll, Liang Qiao



PII: S2588-8420(20)30030-4

DOI: <https://doi.org/10.1016/j.mtnano.2020.100101>

Reference: MTNANO 100101

To appear in: *Materials Today Nano*

Received Date: 17 June 2020

Revised Date: 12 October 2020

Accepted Date: 12 October 2020

Please cite this article as: Gan J., Yu M., Hoyer R.L.Z., Musselman K.P., Li Y., Liu X., Zheng Y., Zu X., Li S., MacManus-Driscoll J.L. & Qiao L., Defects, Photophysics and Passivation in Pb-Based Colloidal Quantum Dot Photovoltaics, *Materials Today Nano*, <https://doi.org/10.1016/j.mtnano.2020.100101>.

This is a PDF file of an article that has undergone enhancements after acceptance, such as the addition of a cover page and metadata, and formatting for readability, but it is not yet the definitive version of record. This version will undergo additional copyediting, typesetting and review before it is published in its final form, but we are providing this version to give early visibility of the article. Please note that, during the production process, errors may be discovered which could affect the content, and all legal disclaimers that apply to the journal pertain.

© 2020 Elsevier Ltd. All rights reserved.

Defects, Photophysics and Passivation in Pb-Based Colloidal Quantum Dot Photovoltaics

--Manuscript Draft--

Manuscript Number:	MTNANO-D-20-00093R2
Article Type:	Review Article
Keywords:	colloidal quantum dots, photovoltaics, multiple exciton generation, non-radiative recombination, defect analysis
Corresponding Author:	Jiantuo Gan CHINA
First Author:	Jiantuo Gan
Order of Authors:	Jiantuo Gan Miao Yu Robert LZ Hoyer Kevin P. Musselman Yan Li Xiaodong Liu Yonghao Zheng Xiaotao Zu Sean Li Judith Driscoll Liang Qiao
Abstract:	Colloidal quantum dots (CQDs) are a class of third-generation materials for photovoltaics (PVs) that are promising for enabling high efficiency devices with potential for exceeding the Shockley-Queisser limit. This is due to their potential to decrease thermal dissipation via multiple exciton generation during charge conversion and collection, which could potentially lead to an increase in the photovoltage or photocurrent in CQD PVs. But despite a predicted upper efficiency limit of 42–44%, the highest power conversion efficiencies of these PVs using PbS CQDs remains at approximately 13% on a laboratory scale. For further improvements, the fundamental recombination mechanisms need to be studied to determine their effects on the open-circuit voltage (V_{OC}) and charge-carrier lifetime as well as the diffusion length of the carriers. Also, surface defect passivation and interface engineering should be studied. In this work, we discuss different pathways for non-radiative recombination losses in PbS CQD PVs, as well as the strategies for reducing these losses by the passivation of the surface and interface defects. We also discuss routes to overcome limits in the diffusion length of the carriers through the engineering of charge transport layers. This work provides routes for the fabrication of highly efficient CQD PVs.
Suggested Reviewers:	Yiqiang Zhan Fudan University yqzhan@fudan.edu.cn He is an expert in photovoltaics. Sining Yun Xi'an University of Architecture and Technology yunsining@xauat.edu.cn He is an expert in photovoltaics
Opposed Reviewers:	
Response to Reviewers:	

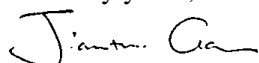
Dear Editor:

Enclosed please find a copy of our revised manuscript “Defects, Photophysics and Passivation in Pb-Based Colloidal Quantum Dot Photovoltaics” by J. Gan, M. Yu, R. L. Z. Hoyer, K. P. Musselman, F. Raziq, Yan Li, X. Liu, Y. Zheng, X. Zu, S. Li, J. L. MacManus-Driscoll and L. Qiao. We would like to submit the manuscript for your consideration as Review in the journal of *Materials Today Nano*.

In the revised manuscript, we have paid attention to the questions and comments listed in the Reviewers’ comments, which leads to a final version of the manuscript.

We look forward to receiving your decision, thank you!

Sincerely yours,

A handwritten signature in black ink, appearing to read 'Jiantuo Gan', written in a cursive style.

Jiantuo Gan

Manuscript Number: MTNANO-D-20-00093

Editor and Reviewer comments:

Editor: please modify the reference format accordingly.
<https://www.elsevier.com/journals/materials-today-nano/2588-8420/guide-for-authors>

Thank you for your comment. In the revised manuscript, we have corrected the format of the references.

Reviewer #2: The subhead in page 9 should be 2.3 XXXX.

Thank you for your comment. In the revised manuscript, we have corrected the subhead.

Defects, Photophysics and Passivation in Pb-Based Colloidal Quantum Dot Photovoltaics

*Jiantuo Gan, Miao Yu, Robert L. Z. Hoyer, Kevin P. Musselman, Yan Li, Xiaodong Liu, Yonghao Zheng, Xiaotao Zu, Sean Li, Judith L. MacManus-Driscoll, Liang Qiao**

Dr. J. Gan, Prof. X. Zu, Prof. L. Qiao
School of Physics, University of Electronic Science and Technology of China,
Chengdu 610054, PRC

M. Yu
State Key Laboratory of Electronic Thin Films and Integrated Devices, University of
Electronic Science and Technology of China, Chengdu 610054, PRC.

Dr. Robert L. Z. Hoyer,
Department of Materials, Imperial College London, Exhibition Road, London SW7
2AZ, UK

Dr. K. P. Musselman
Department of Mechanical and Mechatronics Engineering, University of Waterloo,
200 University Ave. West, Waterloo, N2K 4C8, Canada
Waterloo Institute for Nanotechnology, University of Waterloo, 200 University Ave.
West, Waterloo, N2K 4C8, Canada

Dr. Yan Li
School of Material Science and Engineering, Xi'an Shiyou University, Xi'an 710065,
PRC

Dr. X. Liu, Prof. Y. Zheng
School of Optoelectronic Science and Engineering, University of Electronic Science
and Technology of China (UESTC), Chengdu 610054, PRC

Dr. S. Li
School of Materials Science and Engineering, University of New South Wales,
Sydney 2052, NSW AU.

Prof. J. L. MacManus-Driscoll
Department of Materials Science and Metallurgy, University of Cambridge, 27

Charles Babbage Road, Cambridge, CB3 0FS, UK.

liang.qiao@uestc.edu.cn

Keywords: colloidal quantum dots, photovoltaics, multiple exciton generation, non-radiative recombination, defect analysis

Abstract

Colloidal quantum dots (CQDs) are a class of third-generation materials for photovoltaics (PVs) that are promising for enabling high efficiency devices with potential for exceeding the Shockley-Queisser limit. This is due to their potential to decrease thermal dissipation via multiple exciton generation during charge conversion and collection, which could potentially lead to an increase in the photovoltage or photocurrent in CQD PVs. But despite a predicted upper efficiency limit of 42–44%, the highest power conversion efficiencies of these PVs using PbS CQDs remains at approximately 13% on a laboratory scale. For further improvements, the fundamental recombination mechanisms need to be studied to determine their effects on the open-circuit voltage (V_{oc}) and charge-carrier lifetime as well as the diffusion length of the carriers. Also, surface defect passivation and interface engineering should be studied. In this work, we discuss different pathways for non-radiative recombination losses in PbS CQD PVs, as well as the strategies for reducing these losses by the passivation of the surface and interface defects. We also discuss routes to overcome limits in the diffusion length of the carriers through the engineering of charge transport layers. This work provides routes for the fabrication of highly efficient CQD PVs.

1. Introduction

Solar photovoltaics (PVs) are generating 1.7% of the world's total energy (443 TWh in 2017),[1] and strong growth is predicted for the deployment of PVs over the course of 2017–2023.[2] In order to meet future manufacturing requirements, more viable alternatives to the current wafer-dominated PV market should become available.[1] Emerging PVs are promising, due to their potential for achieving high efficiency at low production costs.[3, 4] For example, colloidal quantum dots (CQDs) have been explored for PV applications since 2002, and are predicted to generate higher photovoltage or photocurrent in PV devices.[5] The reason for an increase in photovoltage is strongly associated with the miniband transport that are formed with the CQD array. In this configuration, the dot-to-dot distance is sufficiently small so that strong electronic coupling takes place and the delocalized quantized miniband states are expected to slow the carrier cooling. Also, long-range electron transport is allowed in the minibands. Namely, the photogenerated carriers are expected to be collected from the miniband structure in the CQD array before they are relaxed to the band-edge. An increase in the photocurrent is expected to occur as a result of additional electron-hole pairs that are generated by the hot carriers, such as through multi-exciton generation (MEG), in which multiple electron-hole pairs (EHPs) are generated upon the absorption of a single photon. MEG is an intrinsic property of CQD absorbers determined as ratio of the absorber's rates for MEG (k_{MEG}) and hot

carrier thermalization (k_{therm}). [5, 6] With MEG, the maximum solar power conversion efficiency (PCE) in solar cells is calculated to surpass the Shockley-Queisser limit to reach ~42–44% if these additional excitons are harvested. [7, 8] At the same time, the synthesis of CQD PVs has a low carbon footprint owing to the low growth temperatures (below 200 °C). [9] These features make CQD PVs an important future source for highly efficient PVs made with low fabrication costs. Moreover, CQDs have a wide range of applications beyond PVs, such as high-performance light emitting diodes and photodetectors, [10] because of their tunable bandgaps as well as high absorption coefficient and photo-luminescence quantum yields (PLQYs). [11, 12] Although PbS CQD PVs contains toxic elements such as Pb that are harmful to the environment, we need to weigh power of the PbS CQD PVs that can provide and the environment issue, which should certainly be tackled at a later research stage with lead free materials for CQD PVs.

PbS CQDs are a leading candidate for MEG, owing to strong quantum confinement being easily achieved due to the large Bohr radius (24 nm). [13-16] In 2010, PbS CQD PVs exhibit PCEs with values of 1.5–3% (**Figure 1a&b**). [13-16] In order to achieve higher PCEs, the loss mechanisms of carriers were investigated. Defect recombination at the PbS CQD surfaces and interface charge recombination [17-21] were identified as the primary limiting factors. [22] Hence, a significant number of strategies for passivating the defects on the surfaces of PbS CQDs have been implemented, leading to successful improvement in the short circuit current densities (J_{sc}) and PCEs in the CQD PVs. [9, 23-33] Also, elimination of the interface defects has been found relevant

for improving the efficiencies via engineering of charge transport layers (CTLs). As a result, the highest PCEs reported to date in PbS CQD PVs have reached over 13%, with a high J_{SC} (~ 28.9 mA/cm²). [34-36] Nevertheless, these devices are limited by a large open circuit voltage (V_{OC}) deficit (0.6–0.8 V), which were not eliminated by the aforementioned strategies of passivation. The V_{OC} deficit is strongly correlated with the non-radiative recombination in the PbS CQD thin films, [22] which indicates that further defect passivation is necessary in order for the V_{OC} s to approach the Shockley-Queisser limit (S-Q limit), let alone exceed it.

In this Review, we study the fundamental mechanisms of carrier generation and recombination in the CQDs as well as their effect in the power conversion efficiencies in CQD PVs. We identify the primary loss mechanisms in CQD PVs and the passivation strategies that are effective at reducing defect recombination via different channels. We also identify future strategies for achieving higher efficiencies in these CQD PVs.

2. Synthesis and Working Principles of CQD PVs

Before we discuss the efficiency losses via different types of defect recombination channels in CQD PVs, it is important to understand the mechanism of MEG in CQDs and its contribution to PCEs breaking the S-Q limit in CQD PVs. In this section, we will concentrate on the synthesis of CQDs, carrier generation in the CQDs by MEG, the mechanism for the increase in PCE, as well as charge transport in the CQD PVs.

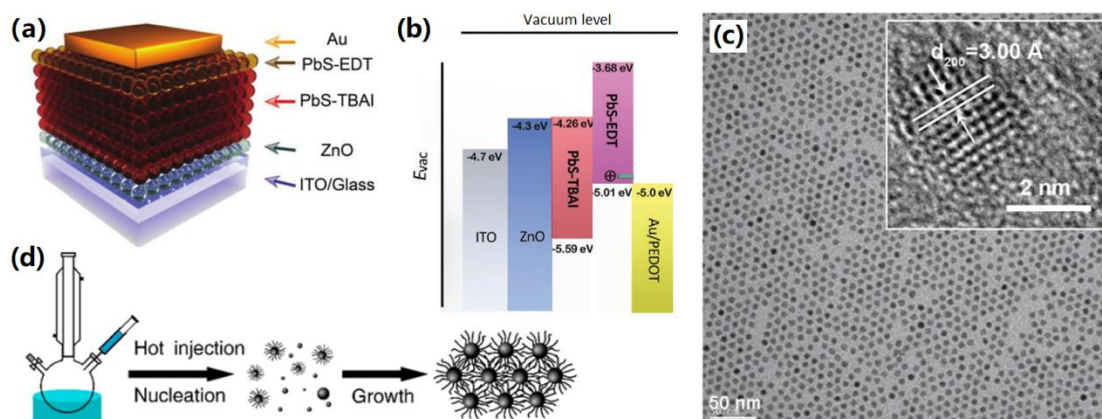


Figure 1. (a) Schematic of a regular structure CQD solar cell. Reproduced with permission.[32] Copyright 2018, Wiley-VCH. (b) Band structure of the CQD solar cell. Reproduced with permission.[37] Copyright 2017, Wiley-VCH. (c) TEM image of PbS QDs. Reproduced with permission.[38] Copyright 2011, Wiley-VCH. The inset shows high resolution TEM image of oleic acid-capped PbS QDs. Reproduced with permission.[39] Copyright 2018, Wiley-VCH. (d) Schematic of CQD synthesis by hot-injection method. Reproduced with permission.[40] Copyright 2015, American Chemical Society.

2.1 Synthesis of CQDs

Typically, CQDs for PVs are required to be mono-disperse, that is have a narrow size distribution (Figure 1c), so that the device V_{oc} could be reduced to achieve high PV efficiencies.[41] This is so that a mini-band structure which is analogous to a 1D superlattice in CQD array with a strong electronic coupling can permit smooth charge transport within the CQD layer.[9, 42] According to the Finke-Watzky theory, this can be realized by the *key separation of nucleation and growth in time* via a subsequent autocatalytic surface growth in hot injection method (Figure 1d).[43] The surface energy of the seeds, degree of super-saturation as well as reaction temperature and reaction time can be adjusted to achieve high mono-dispersity in CQDs.[44, 45] In particular, the surface energy can be altered by the choice of ligands.[46] On the other hand, for dot size, Ostwald ripening and Lifshitz-Slyozov-Wagner (LSW) theory reveals that the high solubility, large surface area and surface energy of the quantum-

size particles allows the growth of large particles.[47-49] The size is also affected by the flux of Pb- and S- precursors injected into the solution as described by Reiss *et al.*[50] By changing the concentration of the Pb- and S- precursors, the shape of the nanocrystals can vary from isotropic dots to spindle-shaped nanocrystals, to rods and other elongated structures.[51] As a result, it is feasible that the desirable CQDs with uniform sizes and shapes can be fabricated by optimization of the synthesis process.

2.2 MEG and PCE in CQD PVs

Unlike bulk materials, CQDs with a large Bohr radius have strong quantum confinement, leading to a splitting of the conduction band (CB) and the valence band (VB) in these CQDs (Figure 2a). The discrete sub-energy levels further enable the generation of multiple electron-hole pairs (EHPs) upon photo-excitation, which is favorable for yielding more photo-generated carriers and higher power conversion efficiencies compared to the conventional thin film solar cells. Hence, CQDs with a large Bohr radius (*e.g.*, PbS) are potentially suitable for the fabrication of CQDs exhibiting MEG for achieving high PCEs beyond the S-Q limit. On the other hand, short dot-to-dot distances in CQD arrays permit strong electronic coupling, thus enabling long-range electron transport within the CQD photoactive layer as long as the CQDs are uniform in size and well aligned.[9, 42] Hence, the CQD array is more efficient as a photo-absorber in the generation of electron-hole pairs compared to bulk materials and has good charge transport properties, making them competitive for

fabrication of highly efficient PVs for the future.

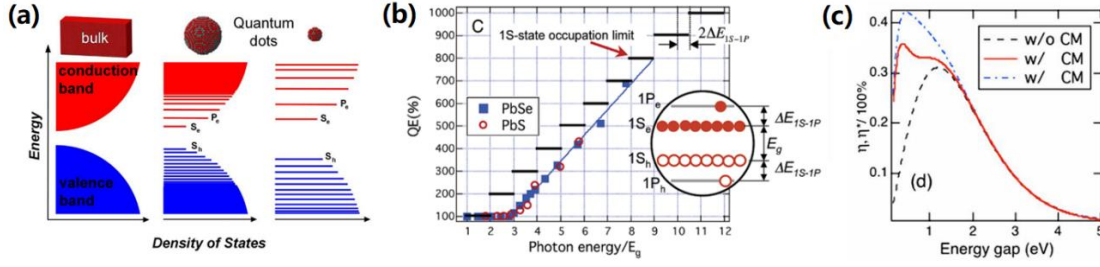


Figure 2. (a) Schematic of size dependent bandgap in CQDs. Reproduced with permission.[52] Copyright 2016, Science Publishing Group. (b) Ideal staircase-like internal quantum efficiency (IQE) derived from energy conservation and IQEs of PbSe, and PbS CQDs, measured as a function of $h\nu/E_g$, along with linear fits with a slope of ca. $100\%/E_g$ and MEG thresholds of $2.5E_g$, $2.85E_g$, and $3E_g$, respectively. Reproduced with permission.[53] Copyright 2006, American Chemical Society. (c) Maximum PCE calculated for different spectral dependences of photon-to-exciton conversion. In the figure, the efficiency is calculated without considering carrier multiplication (CM, equal to MEG) (black dashed line), and with CM with thresholds of $3E_g$ (red solid line) and $2E_g$ (blue dashed line), respectively. Reproduced with permission.[8] Copyright 2006, American Institute of Physics.

Currently, the CQDs using lead chalcogenides (PbX, with X = S, Se or Te) are frequently investigated for their potential in the fabrication of MEG CQD devices, owing to their relatively large Bohr radii (a_B of 24–152 nm[16]) and long diffusion lengths (40–230 nm[9, 54] in the PbS CQD films) enabled by a low effective mass of carriers ($0.09m_e$).[55] As it can be seen, the quantum yield (QY) is strongly dependent on the normalized photon energy ($h\nu/E_g$), which increases linearly after a MEG threshold ($\sim 2.9E_g$), regardless of whether it is PbS or PbSe (**Figure 2b**). The QY in a PbX CQD indicates the number of the EHPs obtained upon absorption of a photon. In order to correlate the QY in a CQD with ultimate PCE that can be achieved in CQD PVs, Klimov *et al.* theoretically investigated the underlying mechanism of efficiency boosts in CQD PVs via the MEG effect. The PCE of a CQD PV is found to be highly dependent on QY of the CQDs. It is predicted to break the S–Q limit and reach 42–

44% as long as the threshold of MEG is reduced to $2E_g$ (Figure 2c).[8] This further suggests that the maximum potential device efficiency is critically determined by both QY via MEG as well as the MEG threshold.[40, 56]

2.3 PbS CQD PVs

To evaluate whether the MEG effect has contributed to the efficiency of the PbS CQD PVs, which has the highest PCE (12.6% [34] vs 10.68% in PbSe [57] and 1.9% in PbTe [16]) among the PbX CQD PVs, we investigated the spectra of internal quantum efficiency (IQE) for these devices. Unlike conventional PV devices, the peak IQE is expected to surpass unity in the long wavelength region (associated with the threshold energy of the MEG effect), indicating that more than one carriers are generated and converted for CQD PVs with MEG. Unfortunately, the peak IQE seldom exceeds unity in the PbS CQD PV devices. By contrast, the peak IQEs for PbSe and PbTe CQD PVs have both exceeded unity (**Figure 3**). The situation remained unclear until several recent reports on PbS CQDs-sensitized solar cells (**Figure 3a&a'**). The absorbed photon-to-current efficiency (APCE) broke unity beyond the point of the MEG threshold.[58] Yan *et al.* have explained it as the interference of the absorption of the TiO₂ or fluorine doped tin oxide layers of the incident photons prior to reaching the CQD layer.[59] As a result, bandgap engineering of the CTLs is needed if more energetic photons are to be absorbed by the PbS CQDs. Because the peak IQEs are observed to be dependent on the normalized bandgap ($h\nu/E_g$) in the CQDs.[60, 61] This suggests that the PbS CQD PVs with a bandgap of 1.3-1.5 eV are conventional heterojunction solar cells rather than MEG solar cells, without multiple electron-hole

pairs contributing to the performance of the CQD PVs.

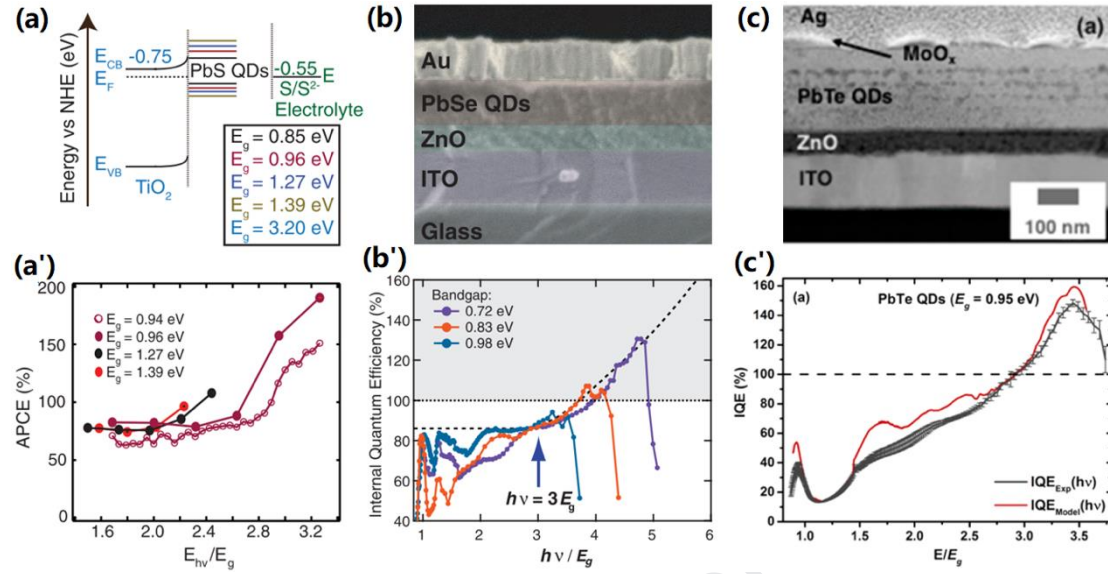


Figure 3. (a) Band energy diagram indicating the relevant energy levels of PbS CQDs (with variously sizes)/TiO₂ as well as the sulfide/polysulfide electrolyte. Reproduced with permission.[58] Copyright 2010, Science Publishing Group. (b) Cross-sectional SEM image of PbSe PV. Reproduced with permission.[60] Copyright 2011, Science Publishing Group. (c) Cross-sectional SEM image of PbTe PV. Reproduced with permission.[61] Copyright 2015, American Chemical Society. (a') APCE versus the incident photon energy divided by the PbS CQD bandgap energy (indicating multiples of the bandgap). Reproduced with permission.[58] Copyright 2010, Science Publishing Group. (b') Collected IQE curves versus the ratio of photon energy to PbSe CQD bandgap, $h\nu/E_g$. Reproduced with permission.[60] Copyright 2011, Science Publishing Group. (c') IQE spectrum of CQD PVs consisting of PbTe CQDs ($E_g = 0.95$ eV). $\text{IQE}_{\text{Exp}}(h\nu)$ and $\text{IQE}_{\text{Model}}(h\nu)$ were determined using reflectance measurements and optical modeling, respectively. Reproduced with permission.[61] Copyright 2015, American Chemical Society.

On the other hand, the shape of the nanocrystals matters in MEG. Studies showed that the QY could be enhanced in PbSe nanorods (NRs) compared to the PbSe CQDs, and PVs based on PbSe NRs have peak external quantum efficiencies of 122% (with the IQE estimated to be higher than 150%).[62] In order to explain the high IQE value in PbSe NRs, Davis *et al.* investigated their PLQYs and found that the rate of MEG increase is slower in CQDs than in NRs, indicating a rapid carrier cooling in PbSe CQDs. Yet, another possible reason could be less efficient charge-carrier generation in

PbSe QDs than in NRs.[62, 63] This alternatively suggests that the shape engineering of the nanocrystals via the synthetic process could provide a second route for harvesting multiple electron-hole pairs for highly efficient CQD PVs.

2.4 Charge Transport

Unlike conventional thin film photo-absorbers, a mini-band structure is analogous to a 1D superlattice in CQD array. It is therefore necessary to investigate the transport mechanism of carriers and carrier recombination as well as to optimize the device structure of CQD array so that the band diagram of CQD PVs is suitable for EHP dissociation and consequently interface extraction[64] and efficient carrier collection.[26, 65, 66]

Based on the Hecht drift-transport model,[54] the carrier extraction efficiency $\eta(V)$ is related to recombination lifetime by Equation 2a:

$$\eta(V) = \frac{\mu\tau_{rec}(V_B - V)}{d^2} \left[1 - \exp\left(\frac{-d^2}{\mu\tau_{rec}(V_B - V)}\right) \right] \quad (2a)$$

where d is the depleted region thickness, μ is the carrier mobility, and V is the external bias. In the study, Kemp *et al.* proposed that carrier extraction efficiency $\eta(V)$ is assumed to be limited by the transport time (τ_t), where carriers suffer from Shockley-Read-Hall recombination (in **Figure 4a**).[54] The transport time and probability of carrier extraction is thus position x -related and given by **Equations 2b&c**:

$$\tau_t = \int_0^x \frac{dx}{\mu E(x) + v_D} \quad (2b)$$

$$P = \exp\left(\frac{-\tau_t(x)}{\tau_{rec}}\right) \quad (2c)$$

where recombination time, τ_{rec} , is defined as the ratio of a carrier's diffusion length

(L_D) to its velocity. This ultimately reveals that the $\eta(V)$ is dependent on diffusion length L_D of carriers, which is correlated with carrier lifetime τ_{rec} , in addition to the carrier mobility μ . As a result, it is favorable to further study the influence of these two factors (carrier lifetime and mobility) on the carrier extraction efficiency of the CQD PVs.

2.4.1 Diffusion length

The diffusion length L_D can be experimentally determined using a PL-based technique assuming the fact that the PL flux is directly related to the diffusion length of carriers. Subsequently, the plot of normalized PL intensity vs distance can be fitted to determine the L_D . [67] At the same time, low-coupling and high-coupling cases are considered, corresponding to different passivation schemes, where the CQDs with oleic acid (OA) ligands corresponds to the low-coupling situation with a short diffusion length, whereas the CQDs with mercaptopropionic acid ligands corresponds to the high-coupling situation with a long L_D . Here, under the framework of a 3D model, L_D also can be calculated as the square root of the diffusion coefficient D and effective time constant:

$$D = \frac{Sd}{\tau_{bandedge}6\sigma} \quad (5a)$$

$$\tau_{effective} \sim \tau_{traps} = \frac{\tau_{bandedge}}{S \times N_t} \pi r^2 \quad (5b)$$

from which L_D is determined to be related to inter-dot distance d . The schematics of charge transport are displayed for two different coupling conditions in **Figure 4c**, where the slope S (PL ratio with acceptor concentration inset of **Figure 4d**), is inversely related to capture cross-section σ and the trap density N_t . From the model,

the trap density N_t can also be determined by calculating PL fluxes measured for different energy levels (the CBs of the CQD donor and intentionally introduced CQD acceptor and trap energy level within the CQD donor, as shown in **Figure 4c**) at different acceptor concentration levels. Further, in **Figure 4e**, the mobility, trap density and L_D are all calculated from the model. Interestingly, a high mobility does not ensure a long diffusion length, but rather the trap related parameters is the crucial parameter in determining the diffusion length.

In addition, the diffusion length can be tripled to ~230 nm through mutual dot-to-dot surface passivation in PbS CQD PVs, leading to an increase in J_{SC} to 29.5 $\text{mA}\cdot\text{cm}^{-2}$ from 21.6 $\text{mA}\cdot\text{cm}^{-2}$ in the control device.[9] This is consistent with the results from previously discussed models. In terms of charge-carrier mobility in CQD thin films, however, experimental values in the range of 8.5×10^{-4} to $2 \times 10^{-2} \text{ cm}^2/\text{V}\cdot\text{s}$ are reported for recently fabricated devices and it means that the mobility should also be improved for its part to contribute to the efficiency according to the theoretically calculated optimized value in Sec.3.[55, 68, 69]

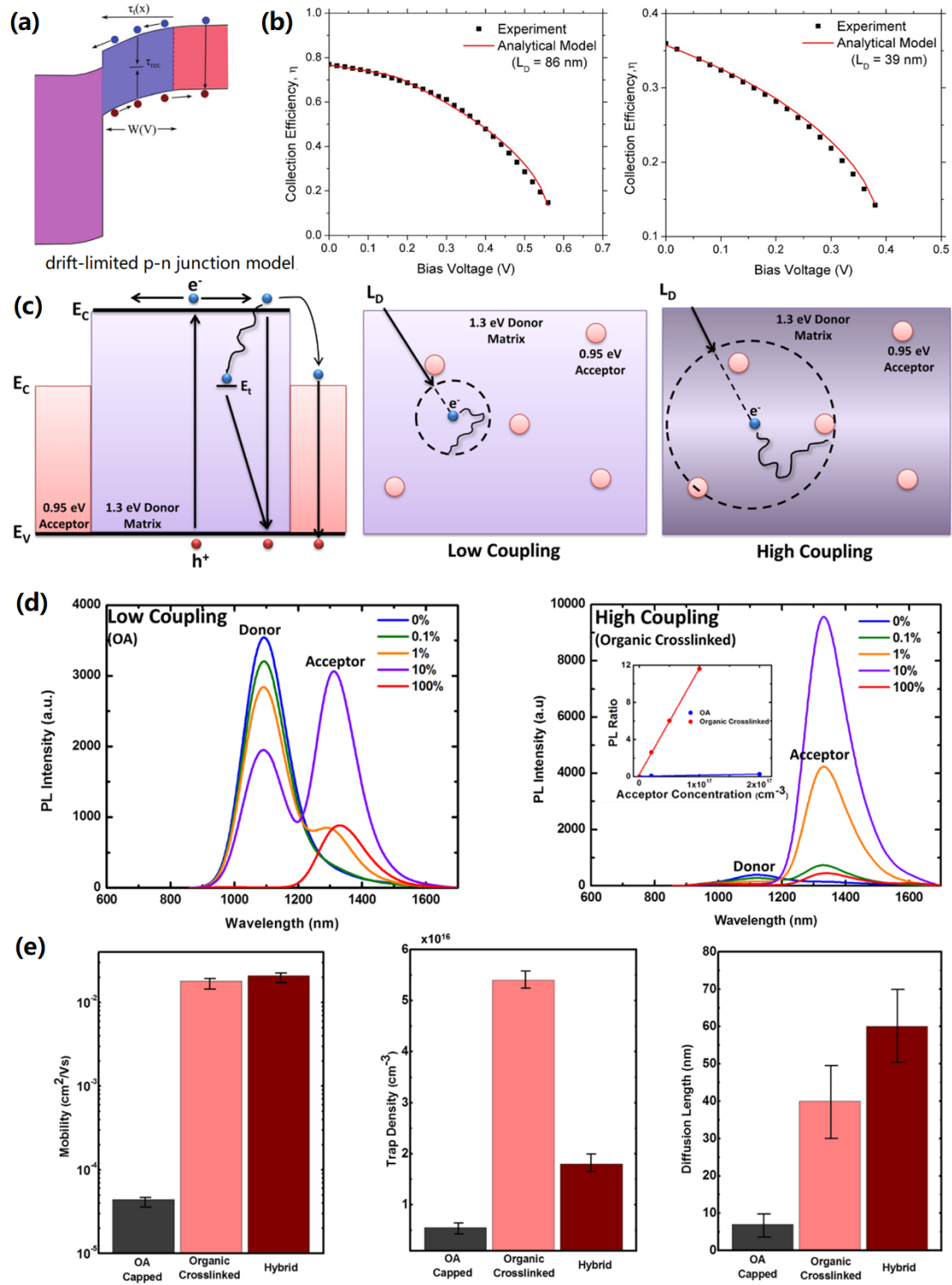


Figure 4. (a) Schematics of drift-limited p - n junction model. (b) Collection efficiency and analytical fit (**Equation 3**) for: hybrid- passivated CQD solar cell and organically cross-linked organic CQD solar cell. Reproduced with permission.[54] Copyright 2013, American Institute of Physics. (c) Energy band diagram of donor and acceptor material and transport and recombination pathways that a charge carrier may undertake when generated in the donor host material; macroscopic depiction of the low-coupling scenario where the average

delocalization of the carrier is small compared to the distance to an acceptor; and high-coupling scenario where the delocalization distance is large and hence the carrier can recombine through acceptor sites. PL spectra for (d) The CQD films with mercaptopropionic acid ligands and with oleic acid ligands with a given percentage of small bandgap inclusions, showing charge transfer under the various coupling regimes. The inset shows sample PL ratios for low (oleic acid ligands) and highly coupled (mercaptopropionic acid ligands) materials as a function of acceptor concentration. (e) Extracted mobility, trap density and diffusion length for several types of PbS CQD solid films.[67]

2.4.2 Mobility

In spite of impressive mobilities achieved in the CQD thin films ($1\text{--}30\text{ cm}^2/\text{V}\cdot\text{s}$), lower mobilities in the range $10^{-3}\text{--}10^{-2}\text{ cm}^2/\text{V}\cdot\text{s}$ have given the best photovoltaic performance for CQD PVs. Because in the mobility-invariant regime, the diffusion length determined by recombination in the space-charge region is found to be ultimately determined by the power conversion efficiency rather than the carrier mobility.[70] **Figure 5a&b** reveals the relation between the important parameters of carrier lifetime and diffusion length and the mobility of the carrier. It can be seen that L_D is increased with carrier mobility while τ_{rec} is decreased with it (in the mobility range of $0.001\text{--}1\text{ cm}^2/\text{V}\cdot\text{s}$). At the same time, both of the parameters are limited by the trap density N_t . However, the diffusion length shows slow variations in the case of high trap density ($N_t > 10^{16}\text{ cm}^{-3}$); The lifetime is in general reduced with an increasing carrier mobility regardless of the trap density.

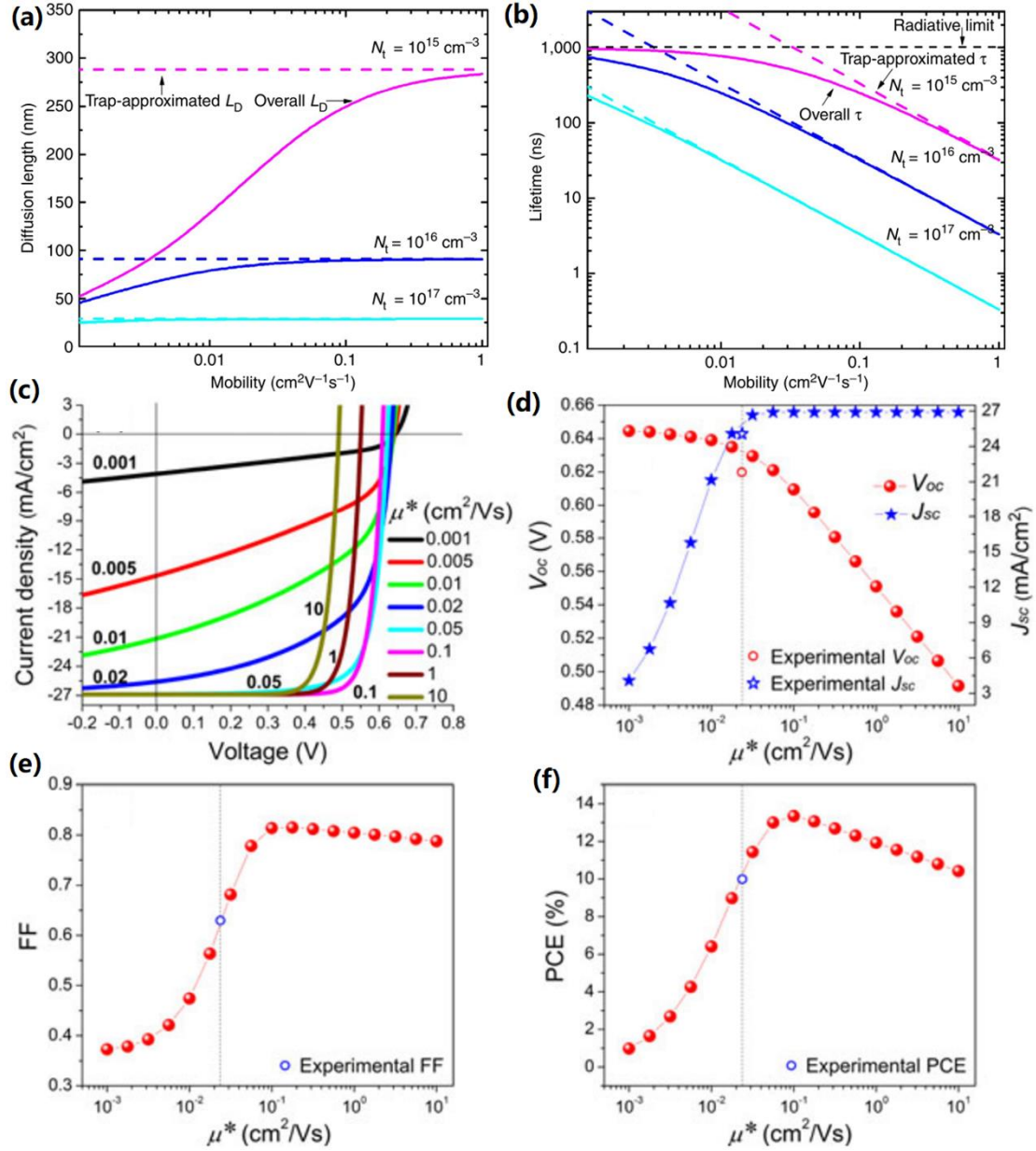


Figure 5. Diffusion length dependence (a) and lifetime dependence (b) on mobility. Reproduced with permission.[55] Copyright 2014, Macmillan Publishers Ltd. (c) Simulated charge-carrier mobility-dependent $J-V$ characteristics; (d) curves of charge-carrier mobility-dependent V_{oc} and J_{sc} ; (e) FF; and (f) PCE.[71] Copyright 2017, Viley-VCH.

Kramer *et al.*[72] have pointed out the importance of charge-carrier mobility from the CQD PV point of view. With band-edge electron mobility being $0.03 \text{ cm}^2/\text{V}\cdot\text{s}$ for both electrons and holes in the CQD thin film, 6% in PCE can be obtained in the device.[24] When the mobility is increased to $0.1 \text{ cm}^2/\text{V}\cdot\text{s}$ and $0.4 \text{ cm}^2/\text{V}\cdot\text{s}$, the PCE

is predicted to reach 10% and 15%, respectively. In order to elaborate the influence of charge-carrier mobility on device efficiency, a carrier-hopping drift diffusion model has been set up for evaluation of carrier mobility and its effect on the J - V characteristics.[71] As shown in **Figure 5c-f**, J_{SC} increases substantially from 3 to 27 $\text{mA}\cdot\text{cm}^{-2}$ when carrier-hopping mobility is varied from $0.001\text{ cm}^2/\text{V}\cdot\text{s}$ to $10\text{ cm}^2/\text{V}\cdot\text{s}$. However, the V_{OC} is reduced from 0.6 V to 0.5 V. The V_{OC} loss is mainly from the dark carrier recombination. At high mobilities, the dark carriers from the electrode diffused rapidly to recombine with the photo-carriers.[73, 74] In the end, the optimal mobility is estimated to be $0.1\text{ cm}^2/\text{V}\cdot\text{s}$.

As a result, from the point of view of charge transport, the PCE of CQD PVs is strongly influenced by both the diffusion length of the carriers, which depends on charge-carrier lifetime and mobility. In comparison with the mobility, trap-related parameters such as charge-carrier lifetime are strongly associated with the diffusion lengths. By contrast, the mobility does not affect the PCE of CQD PV as long as they reach certain values ($0.1\text{ cm}^2/\text{V}\cdot\text{s}$), thereafter a higher mobility in CQD array decreases the PCE of the CQD PVs. Therefore, trap related recombination in CQD PVs should be suppressed in order to achieve higher efficiencies.

3. Fundamental Loss Mechanisms

Non-radiative recombination has a significant impact on the diffusion lengths of carriers, which influences the PCEs of CQD PVs. In this section, we will investigate different pathways of defect recombination and summarize passivation methods that can lead to efficiency improvements in PbS CQD PVs.

3.1 Sub-bandgap defects

The efficiencies of PbS CQD PVs are shown to be strongly limited by a large V_{OC} deficit (0.6–0.8 V) with a bandgap (1.2–1.4 eV) of the PbS CQD layer (**Figure 6a**). Typically, the V_{OC} deficit is correlated with defect recombination via sub-bandgap defects, which are originated from the unsaturated dangling bonds, vacancies and interstitials at the surface of the PbS CQDs (**Figure 6b**), owing to a large surface-to-volume ratio in these CQDs.[40] These traps are located between the sub-energy levels ($1S_e$ and $1S_h$) within the bandgap and act as unfavorable centers for capturing the photo-generated carriers. Fortunately, these defect energy levels can be pushed outside the PbS bandgap using passivating methods (**Figure 6b**), via interaction between the surface atoms of the PbS CQDs and the ligand molecules, which are shown to effectively improve the PbS device efficiencies. In addition, the V_{OC} deficit is affected by Urbach energy in the PbS CQDs solids,[75] in which higher Urbach energies correlate with increased disorder and longer band-tails extending from the band extrema that lead to increased thermalization of photogenerated carriers. Typically, the Urbach energies are 22–38 meV for PbS CQD films (with bandgaps of 1.2–1.4 eV, which are typically used for fabrication of PbS CQD solar cells), yielding

a V_{OC} deficit of $\sim 0.35\text{--}0.6$ V and theoretical efficiency limit of 31%. However, the Urbach energy for the PbS CQD films were measured to be 22–24 meV by photothermal deflection spectroscopy after they are passivated with molecular ligands EDT and TBAI, which makes the V_{OC} and theoretical efficiency limit to be free from the effect of Urbach energies as long as these PbS CQDs are properly passivated in the leading devices. On the other hand, the V_{OC} deficit is also associated with the photoluminescence quantum yield (PLQY) in PbS CQDs.[76] The PLQY is improved together with the V_{OC} deficit being reduced for the PbS device when surfaces of the PbS CQDs are passivated. The PLQY could also be improved via surface modification of other CQDs using bi-inorganic ligands rather than conventional organic ligands, which leads to an increase in the carrier conductivity as well as carrier injection rate.[77] Therefore, surface passivation is vital in improving the V_{OC} deficit in the PbS CQD devices through reductions of surface trap recombination and Urbach energy with increase of PLQY in the PbS CQDs.

In order to understand the underlying mechanism of carrier capture by the sub-bandgap defects, ultrafast transient absorption spectroscopy (TAS) is effective in determining the carrier lifetime in PbS CQDs ($\sim 10\text{--}100$ ps for biexcitons, Figure 6c),[78] but this technique is unable to further explain the energy levels of these sub-bandgap defects. For further study, an electro-optical technique, pump-push photocurrent spectroscopy, was employed to study PbS CQD PV devices. It was found that the IR photo-induced absorption of PbS CQDs in the 0.2–0.5 eV region is partly associated with immobile charges. [79] At the same time, the early trapping

dynamics were observed to strongly rely on the surface-modifying ligands, indicating that the carriers recombine through immobile charges in a similar way to surface-defect-related recombination. Surface defect passivation through ligand exchange has been found helpful in passivating these charge-active defects, resulting in improvement in J_{SC} as well as PCE in CQD PVs.[54] Therefore, the passivation of defects with traps 0.2–0.5 eV from the band-edge through surface ligand exchange is an effective way for improving the device performance of CQD PVs.

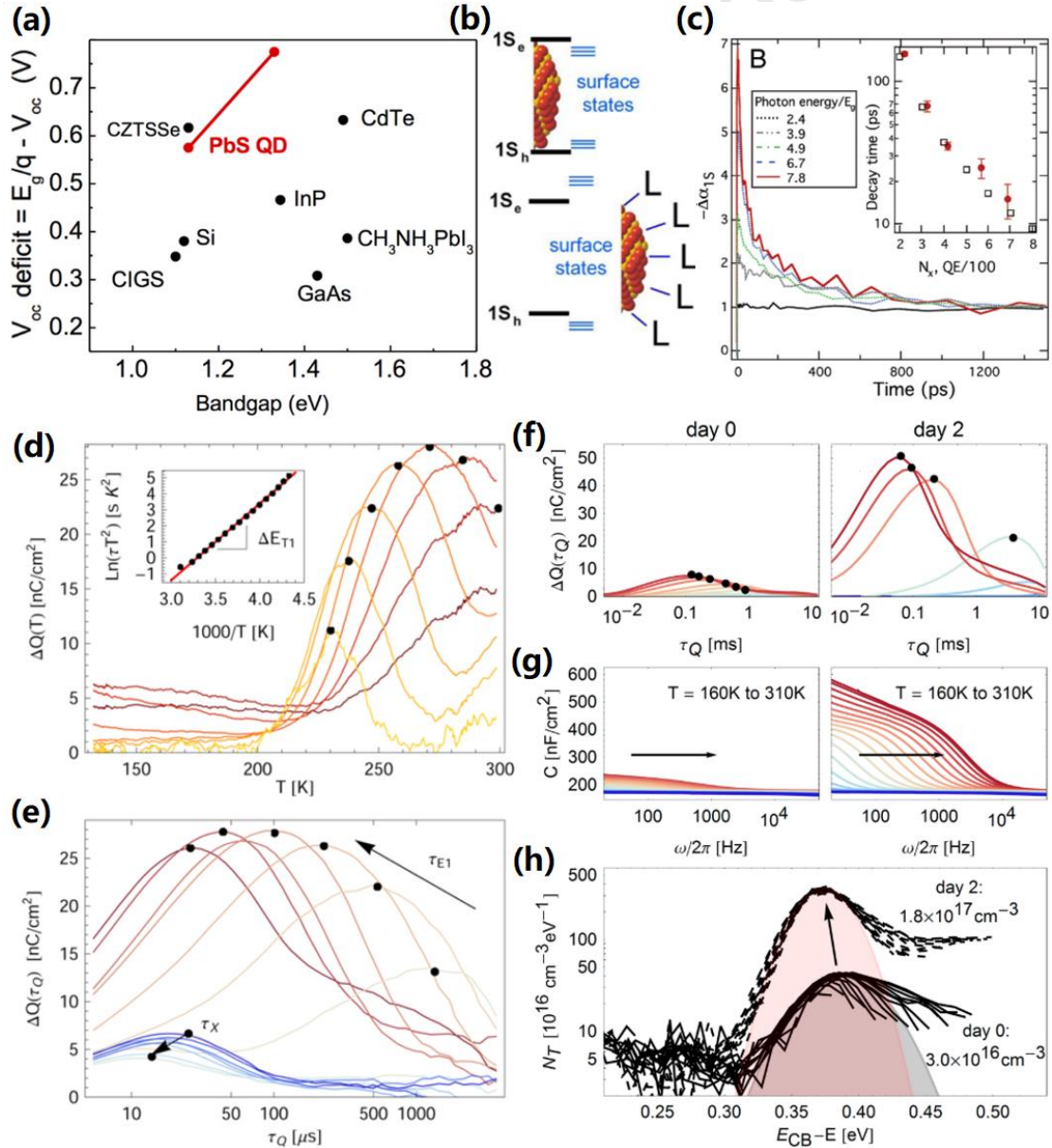


Figure 6. (a) The V_{OC} deficits in PbS CQD PVs (with two PbS bandgaps shown) and other common PV materials. V_{OC} values correspond to certified record-efficiency devices. Reproduced with permission.[22] Copyright 2015, American Chemical Society. Copyright 2016, Science Publishing Group. (b) Dangling bonds at the CQD surface and their energy states within the bandgap. Altering the energy level of the surface states, i.e. pushing them outside the bandgap, by manipulating the interaction between the QD surface atoms and ligand molecules. Reproduced with permission.[52] (c) TA traces recorded for different pump photon energies (from 2.4 to $7.8E_g$). Inset: multi-exciton lifetimes calculated using the $(N_x)^2$ scaling (black open squares) and initial decay constants measured from traces recorded in the regime of CM (red solid circles). Reproduced with permission.[53] Copyright 2006, American Chemical Society. (d) Deep level transient spectroscopy plots of ΔQ versus temperature (T) for different detector time constants (τ_Q). The Arrhenius plot in the inset relates the temperature at which the peak in ΔQ occurs to the corresponding τ_Q . (e) The same spectra (ΔQ) as in (a) plotted versus τ_Q for temperatures between 131 K (blue) and 300 K (red). The thermally activated emission time constant (τ_{EI}) is clearly visible. Reproduced with permission.[80] Copyright 2013, American Chemical Society. (f) Current-based deep level transient spectroscopy spectra on the device immediately after fabrication and after storage in air for two days. (g) Thermal admittance spectroscopy data for an applied bias voltage of 0 V. (h) Trap state density (N_T) determined by thermal admittance spectroscopy. Reproduced with permission.[81] Copyright 2013, American Chemical Society.

On the other hand, to further calculate the density of these sub-bandgap defects, electrical measurements are employed to analyze the PbS CQD PVs. Using Shockley-Read-Hall (SRH) and Walter models, investigations of recombination mediated by sub-bandgap defect states in CQD PVSs are undertaken via current-based deep level transient spectroscopy (Q-DLTS) (Figure 6d&e) and impedance spectroscopy (Figure 6f-h).[80, 81] Through the Q-DLTS study, Bozyigit *et al.* have pointed out the deep-lying traps with an activation energy of 0.40 eV from the CB with a density N_T of $1.7 \times 10^{17} \text{ cm}^{-3}$ exist in ethanedithiol (EDT)-treated PbS devices (**Table 1**). In this study, current flowing through the device has a certain theoretical relation with the emission time constant of the defect. As a result, N_T was extracted from the integral of the measured current and at the same time the activation energy of the defect was

deduced from the transient current. In addition, using the Walter model combined with impedance spectroscopy measurement, the measured capacitance of the SCR and its relation with measurement frequency helped to determine the N_T to be $1.8 \times 10^{17} \text{ cm}^{-3}$ with an activation energy of 0.36 eV below the N_C (**Table 1**). In order to improve the efficiency of the PbS CQD PVs, these sub-bandgap defects should be passivated with surface modification using ligand molecules.

Table 1. Summary of trap information using different techniques.[82]

PCE %	J_{sc} mA/cm ²	V_{oc} V	FF %	Method	Trap density	Trap energy eV	Year and Ref.
2.3	9.7	0.47	51	Q-DLTS	$1.7 \times 10^{17} \text{ cm}^{-3}$	0.4 below CB	2013[80]
2.25	8.67	0.5	51.5	Impedance spectroscopy	$1.8 \times 10^{17} \text{ cm}^{-3}$	0.36 below CB	2013[81]
9.41	25.0 ^{a)}	0.67 ^{a)}	26.0 ^{a)}	Impedance spectroscopy	$3.2 \times 10^{16} \text{ cm}^{-3} \cdot \text{eV}^{-1}$	0.34 below CB	2016[82]

a) Here only the first three effective numbers are considered.

3.2 Interface Defects

Apart from the sub-bandgap defects in PbS CQD surfaces, recombination at the interfaces between the active layer and charge transport layers need to be addressed.[83] Instead of being located at a fixed energy level as for the sub-bandgap defects, they have a continuous distribution along the energy levels, which is similar to the tail states in CTLs (**Figure 7a**).[84] Hence, carriers are trapped with this type of defects at various energy levels, which will be distinguished from the sub-bandgap defects in the decay timescales. The ultrafast charge separation at the hetero-interface are occurring at a timescale faster than sub-bandgap defects.[21] They should also be eliminated from the CQD PV devices.

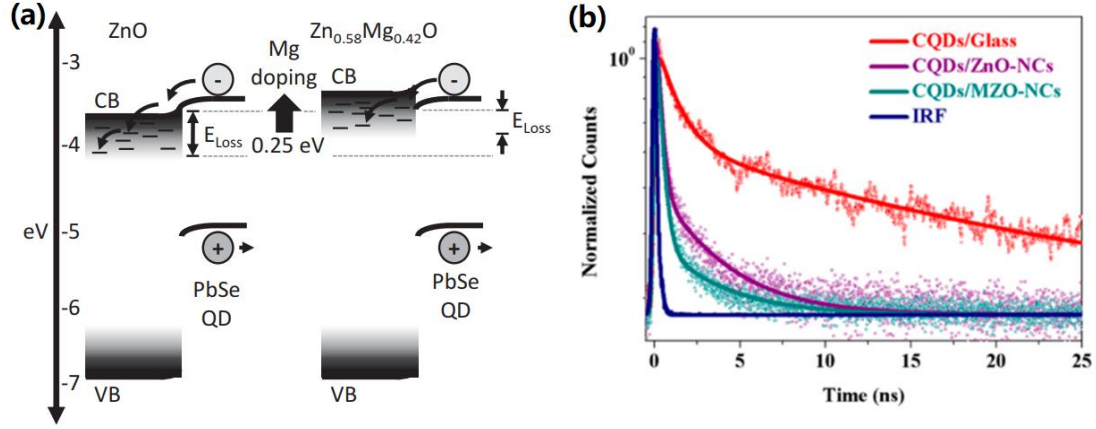


Figure 7. Illustration of the thermalization of electrons transferred from the PbSe QDs to the $\text{Zn}_{1-x}\text{Mg}_x\text{O}$ in devices with $x = 0$ (left) and $x = 0.42$ (right).[85] Copyright 2014, Wiley-VCH. (b) Time-resolved PL decay of CQD solids grown on the ZnO and MZO, respectively. Reproduced with Permission.[86] Copyright 2017, American Chemical Society.

Similarly to the PbS CQDs, the photo-excited carriers in PbSe CQDs are first injected into the ZnO and then thermalize down the tail of states, resulting in an energy loss (E_{loss}) of electrons (**Figure 7a**).[85] Raising the tail through Mg doping in ZnO can reduce the loss. In order to study photo-generation, carrier dynamics have been observed by time-resolved photo-luminescence (TRPL),[87] so that the lifetime of the photo-generated carriers can be determined (**Figure 7b**). The PL intensity decay $I(t)$ can typically be fitted to a bi-exponential model using **Equation 4a**:

$$I(t) = A_1 \exp\left(-\frac{t}{\tau_{\text{rec1}}}\right) + A_2 \exp\left(-\frac{t}{\tau_{\text{rec2}}}\right) \quad (4a)$$

where A_1 and A_2 are amplitudes of the emission intensity for two different lifetime components τ_{rec1} and τ_{rec2} . From **Equation 4a**, the two components for carrier recombination can be de-convoluted; namely, the fast decay and the slow decay.

Recombination on different timescales is usually related to different energy levels for relevant traps.[79] Deep-level ($\sim 0.3\text{--}0.5$ eV) trapping centers are relatively slow (on the scale of 10 ns) for carrier capture; whereas shallow traps are closer to the

valence band (~ 0.2 eV) (in the time scale of \sim ps). An average lifetime $\langle \tau_{\text{rec}} \rangle$ can be obtained using the following **Equation 4b**: [87]

$$\langle \tau_r \rangle = \frac{A_1 \tau_{\text{rec}1} + A_2 \tau_{\text{rec}2}}{A_1 + A_2} \quad (4b)$$

In general, the average lifetime $\langle \tau_{\text{rec}} \rangle$ can be altered in CQD PVs depending on their processing methods. [83, 88-90]

In addition, electro-chemical impedance spectroscopy (EIS) was employed to investigate the recombination resistance and carrier lifetime of the PbS CQD PVs. Using EDT ligand modified PbS CQDs as a hole transport layer (device B in Figure.8a-b), the PbS CQD PVs exhibit similar Nyquist plots with a single semi-circle under different forward biases compared with the device without the PbS-EDT layer (device A). However, both the recombination resistance (Figure.8c), which is determined as the cross-section point of imaginary part of the impedance with the x -axis in the Nyquist plots, and lifetime (Figure.8d), which is determined as the value corresponding to the frequency where the imaginary part of the impedance reaching the maximum point in the plot of the frequency dependent imaginary part of the impedance, are higher in the device B with the PbS-EDT hole transport layer under the forward biases (0–500 mV). [65] A large recombination resistance and long carrier lifetime means low carrier recombination losses in device B with PbS-EDT layer. [65, 91] Therefore, the additional charge transport layer is necessary for improving the charge-carrier lifetime while reducing charge recombination loss and improve the efficiency in PbS CQD PVs.

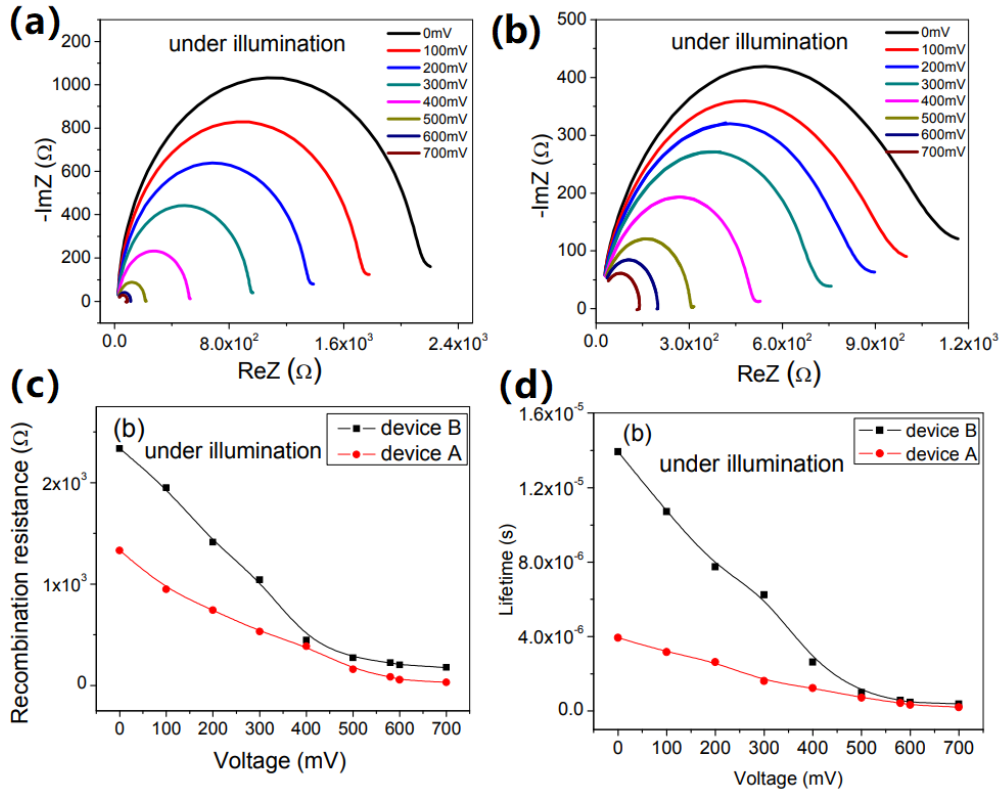


Figure 8. (a) Impedance spectra for the two typical PbS CQDs-based solar cells (a) device B with PbS-EDT layer and (b) device A without PbS-EDT layer at different applied voltages under illumination. (c) The recombination resistances for the two PbS solar cells at various biases under illumination and (d) The carrier lifetime for the two typical PbS CQDs-based solar cells at various biases under illumination. Reproduced with permission from Ref.[65] Copyright 2017, American Chemical Society.

Control over band offsets[17, 92] and ?? doping of the CTLs[93] have proven effective in enhancing interface charge dissociation and reducing interfacial trap state densities. Both recombination resistance and carrier lifetime have been increased for the device with an additional EDT ligand passivated CQD layer as hole transport layer. At zero bias, in particular, the device exhibited an increased carrier lifetime from 4 to 14 μs under AM 1.5 illumination, leading to a leap of PCE from 5.23% to 7.85% [65] (here it should be noted that the carrier lifetime was determined from interface recombination study at PbS CQD/Au interface using EIS, which is not comparable with the carrier lifetime (in pico-second scale) measured in CQDs using

TRPL).

4 Recent Progress in CQD PVs

After we have studied different recombination pathways in PbS CQD PVs, in this section, we will discuss the main strategies that have been implemented for treating both the sub-bandgap and interface defects through surface modification of the PbS CQDs as well as engineering of the CTLs, respectively.

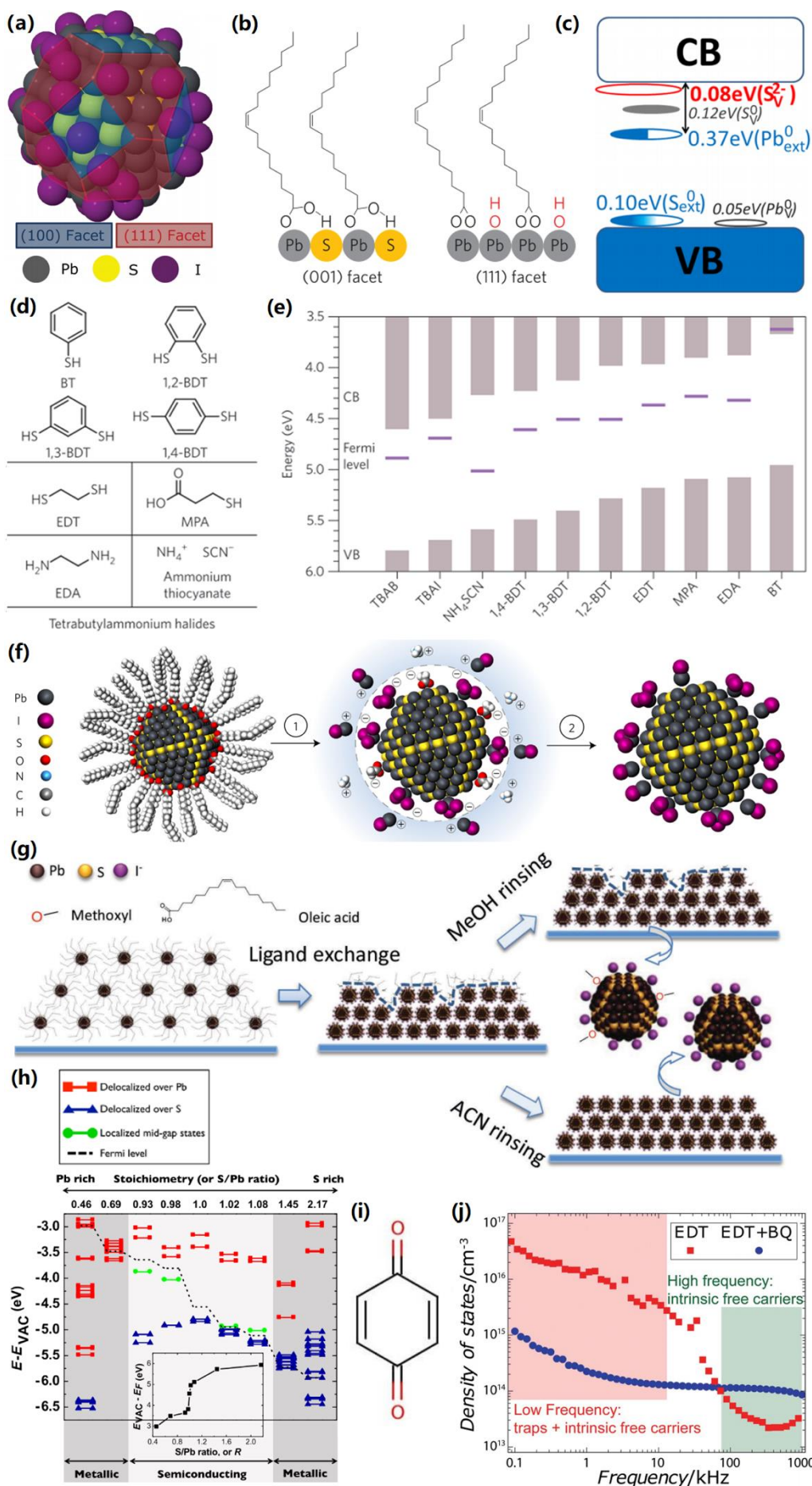


Figure 9. (a) Schematic of atomic structure model of PbS CQDs. Reproduced with permission.[94] Copyright 2015, Wiley-VCH. (b) Schematic of the PbS CQDs with the (001) facet stabilized by oleic acid and the (111) facet with deprotonated oleic ligands together with hydroxide groups. Reproduced with permission.[95] Copyright 2016, Macmillan Publishers Ltd. (c) Schematic of defect energy levels in band structure of PbS CQDs. Reproduced with permission.[96] Copyright 2015, American Chemical Society. (d-e) Energy levels of PbS CQDs with different choice of surface ligands, including: tetrabutylammonium bromide (TBAB); tetrabutylammonium iodide (TBAI); benzenedithiol (BDT); ethanedithiol (EDT); mercaptopropionic (MPA); ethylenediamine (EDA); and benzenethiol (BT). Reproduced with permission.[97] Copyright 2016, Macmillan Publishers Ltd. (f) Solution-phase ligand exchange with metal halide precursors and purified with ammonium acetate. Reproduced with permission.[98] Copyright 2017, Macmillan Publishers Ltd. (g) Schematic diagram of rinsing by two different solvents (acetonitrile and methanol) and their effect on the film morphology.[32] Copyright 2018, Wiley-VCH. (h) Kohn-Sham energy levels for PbS CQDs for different S/Pb stoichiometry. Reproduced with permission.[99] Copyright 2013, American Institute of Physics. (i) Molecular structure of 1,4-benzoquinone (BQ). (j) Density of states for PbS-EDT CQD thin films with and without the BQ treatment.[94] Copyright 2015, Wiley-VCH.

4.1 Surface Modification of the PbS CQDs

Before we proceed to the surface modification of the PbS CQDs, the chemical origin of the surface defects should be identified in addition to the energy level and trap density of the sub-bandgap defects that have been studied in Sec.3.1. In the crystal structure of the PbS CQDs, the stoichiometry between the two chemical elements (Pb and S) is critical in determining whether the PbS nanocrystals are terminated with Pb {111} polar facets or with {100} non-polar facets (Figure 9a).[94, 99] The reason for studying the terminating facet in PbS CQDs is that the chemical origin of the sub-bandgaps in PbS is strongly related to {111} polar facet (Figure 9b). For the as-synthesized PbS CQDs, the {100} facets are stabilized by the covalently binding OA ligands. Whereas, the {111} facets are stabilized by deprotonated oleic acid $[OA]^-$ along with hydroxyl ligand $[OH]^-$ to preserve overall charge neutrality and

minimize surface energy.[95] However, the OA ligands together with $[\text{OH}]^-$ are identified to be the main cause of the sub-bandgap states for the $\{111\}$ polar facets.[31, 95] Besides, the insulating long chain OA ligands produced a barrier for efficient transport within CQDs.[15, 24, 100] On the other hand, the polar $\{111\}$ surface is more prone to atomic reconstruction, forming different types of sub-bandgap defects (S_V^{2-} , S_V^0 , Pb_ext^0 , S_ext^0 and Pb_V^0) with energy levels sensitive to the local stoichiometry (**Figure 9c**).[96] Among these defects, Hwang *et al.* have particularly identified that the chemical origin of another major sub-bandgap states in the PbS CQDs to be the under coordinated Pb atoms (Pb_ext^0 in **Figure 9c**), which are located 0.37 eV below the CB. Therefore, it is necessary to treat the $[\text{OH}]^-$ and Pb_ext^0 before the efficiency of the PbS CQD PVs are improved with an increase in the V_OC .

Table 2 lists a variety of ligands used for surface passivation, with the device efficiency and $J-V$ characteristic parameters achieved for these solar cells. Among the $J-V$ characteristic parameters, J_SC has in particular shown a leap from 8.93 to 31.9 mA/cm^2 .

Table 2. List of PCEs and selected parameters for PbS CQD PVs, their structure and stability improved by CQD surface passivation. ^{a)}

	η %	V_OC V	J_SC mA/cm^2	FF %	p - n Structure	Stability	Year and Ref.
Surface Modification	2.94	0.59	8.93	56.0	PbS/ZnO	1,000 h	2010 [14]
	-	-	-	-	electrolyte/PbS / TiO_2	-	2010 [59]
	5.54	0.53	18.0	59	PbS-CTAB/ TiO_2	-	2011 [24]
	7.4	0.59	21.8	58	PbS-PbCl ₂ /PbS-CdCl ₂ / TiO_2 /ZnO	two weeks	2012 [25]
	8.55	0.55	24.2	63.8	PbS-ETD/PbS-TBAI/ZnO	150 days	2014 [26]
	9.2	0.55	30	58	Mutually passivated PbS-RNH ₂ -Cl/ TiO_2	-	2015 [9]
	9.9	0.64	22.3 ^{a)}	72.4	PbS-I ₂ -ETD/PbS-I ₂ -TBAI/ZnO	-	2015 [101]
	10.5 ^{a)}	0.65	22.5	71	PbS-I-EDT/PbS-I-EMII/ZnO	-	2016 [102]

10.6	0.61	24.3	71	PbS-EDT/PbS _{MAI} -TBAI/ZnO	-	2016 [103]
7.11	0.46	28.3	54.3	PbS/ZnO NW/ZnO	-	2017 [90]
9.7	0.52	31.9	60	PbS-ETD/PbS-TBAI/ZnO NWs/ZnO	3 months	2016 [27]
7.89	0.49	31.0 ^{a)}	51.9	PbS-EDT/PbS-TBAI/TiO ₂	>110 days	2017 [28]
7.6	0.5	27.0	51	MoO ₃ /PbS-EDT(NaHS doping)/PbS-TBAI/TiO ₂	-	2017 [104]
9.58	0.59	24.6 ^{a)}	66	PbS-ETD/PbS-TBAI/ Au BPs@SiO ₂ or Au NSs@SiO ₂ /ZnO	-	2017 [105]
8.95	0.61	21.8	67.9	PbS-EDT/PbS-MAPbI ₃ /ZnO	-	2017 [106]
10.5 ^{a)}	0.65 ^{a)}	23.7 ^{a)}	68.5 ^{a)}	PbS(I in EtOH)-ETD/PbS(I in EtOH)-TBAI/ZnO/ITO	-	2017 [29]
10.2	0.65	24.8	63	PbS-EDT/PbS-ink/ZnO	-	2017 [30]
11.0	0.68	24.1	67	HAL/PbS-PDMII/ZnO	270 days	2017 [31]
11.2	0.63	25.8	68.8	PbS(ACN)-ETD/PbS(ACN)-TBAI/ZnO	-	2018 [32]
10.6 ^{a)}	0.62	25.3 ^{a)}	67.7 ^{a)}	PbAc-PbS-ETD/PbAc-PbS-TBAI/ZnO	-	2018 [33]
9.7	0.53	27.7	65.7	NiO/PbS-EDT/PbS-I/ZnO	-	2018 [107]
12.6	0.64	28.9	68.4	PbS-EDT/Matrix-protected PbS/ZnO NPs	-	2019 [34]

^{a)} Here only the first three effective numbers are considered.

In order to passivate the defects, surface modifications by ligand exchange (molecules structures and induced band level changes in **Figure 9d&e**), [9, 24-26, 98, 101-103, 106, 107] doping, [104] and solvent treatment [29, 32, 33] to passivate the surface defects have proven to be the most effective ways to improve the power conversion efficiency in the PbS CQD PVs. [108] For example, a hybrid PbS CQD ink ligand exchange by PbX₂/ NH₄Ac (ammonium acetate) was shown to maximize the amount of halides on the PbS CQD surface while removing the [OH]⁻ containing OA molecules from the solution (**Figure 9f**). In details, the OA ligands are exchanged by [PbX₃]⁻, so that the PbS CQD surface is stabilized by both [PbX]⁺ and [NH₄]⁺. After centrifuge and precipitation of the PbS CQDs, NH₄Ac is also removed without any undesirable organic residues left. [98] Another example, PbS CQDs treated by a novel iodide based ligand, 1-propyl-2,3-dimethylimidazolium iodide (PDMII) (PbS-PDMII)

demonstrates improved surface properties with reduced sub-bandgap trap-states in comparison with that in PbS-TBAI. The improved surface properties in PbS-PDMII are further shown by an enhanced charge extraction with a diminished energy loss at the energy level of 0.45 eV. As a result, the PDMII treated PbS CQDs devices have reached a certified efficiency of 10.89% with good air-stability (drop to 9.8% after 270 days in air).[31] Furthermore, ligand exchange could also alter the Fermi level of the modified PbS CQD layer (**Figure 9e**), and this opens up the opportunities for band alignment engineering for the PbS CQD PVs.

On the other hand, surface modification of the PbS CQDs using ligand exchange might lead to the treated surface susceptible for oxidation and thus becomes the new traps. For example, passivation of PbS CQDs using halide ions was found to etch the PbS CQD surface, leaving the unpassivated sites open, which will become a new type of surface trap and were also susceptible to oxidation. To solve this problem, a multi-step surface passivation by halides, EDT and Cd is shown to reduce the etching effect by the halide ions. Because the Cd atoms are more easily etched from the surface as compared to the Pb atoms, so that the Pb atoms are protected with less open sites during the ligand exchange.[109] Another soft surface treatment method is shown to realize better performance in PbS CQD devices by using acetonitrile as the rinsing solvent after ligand exchange due to the aprotic nature of acetonitrile (in **Figure 9g**). This results in fewer trap states being introduced during the rinsing process compared to the conventional rinsing solvent methanol.[32] Furthermore, optimization of the PbS CQDs could be by using another soft method in producing PbS CQDs, so as to

give reduced sub-bandgap states. Although studies contradict that the maximum PCE in PbS CQDS PVs is severely dependent on the band tails,[75] it was found that the band tail of the trap distribution becomes narrower as the nanocrystals become larger.[110] Therefore, band tail of the trap distribution by CQD size control provides another possible soft method for reducing trap recombination in PbS CQDs.

In order to further explore the soft methods that are favorable in reducing defects in PbS CQDs, optimization of the synthesis process of PbS CQDs could provide new insights without introduction of new traps as by halide exchange process. **Figure 9h** gives semiconducting properties with varied bandgap and vacuum levels in the limited S/Pb ratio (0.93–1.08). At lower ratios, the sub-bandgap states are located closer to the CB, whereas these states are located closer to the VB once the ratio is higher than 1. Therefore, it is necessary to adjust the synthesis process with S/Pb ratio staying at the ratio of 1:1, so that the surface sub-bandgap traps are minimized. This study provides a new route to achieve high efficiencies in PbS CQD-based solar cells by adjusting the stoichiometry ratio of PbS CQDs. Using *ab initio* calculations, Zhrebetskyy *et al.* have further shown that the PbS CQDs tend to maintain their electronic stoichiometry regardless of the various possible non-ideal atomic configurations, which further indicates that atomically non-stoichiometric PbS quantum dots probably have a clean band gap as long as they satisfy electronic stoichiometry.[96] Moreover, it was discovered that treating with the mild oxidizing agent, 1,4-benzoquinone (see **Figure 9i**) can re-oxidize the under-coordinated Pb atoms, increasing the S/Pb atomic ratio and suppressing trap emission. Then, drive-

level capacitance profiling quantitatively showed that it achieves a 40-fold decrease in trap density (**Figure 9j**).[94] Few studies have been implemented on this, thus we propose that optimization of the PbS CQD synthesis should be studied for producing PbS CQDs without sub-bandgap defects while avoiding introduction of new traps during the halide exchange process.

4.2 Engineering of charge-transport layers

The interface defects that are located at the hetero-interface as well as the back contact[83] act as another major pathway of non-radiative recombination and result in a reduction in V_{OC} and PCE.[111, 112] In the ZnO CTL, interface defects can vary from oxygen vacancies, zinc vacancies, zinc interstitials and/or oxygen interstitials,[113-115] or even due to carbon residuals.[116] These interface defects not only induce trap-assisted interfacial carrier recombinations,[117, 118] but also reduce the electron mobility and worsen charge transport.[116, 119-123] A spike at the heterojunction can also reduce the charge transport.[17] Therefore, passivation of these interface defects is important for achieving high efficiencies in PbS CQD PVs, including engineering of the CTLs via doping,[21] replacement by SnO_2 ,[116] thermal treatment,[30] and chemical modification at the back contact (**Table 3**).[110]

Table 3. List of PCEs and selected parameters for PbS CQD PVs, their structure and stability improved by transport layers as well other techniques. ^{a)}

	η %	V_{OC} V	J_{sc} mA/cm ²	FF %	<i>p-n</i> Structure	Stability	Year and Ref.
[110]	3.5	0.65	8.5	52	MoO ₃ /PbS/TiO ₂ NPs	-	2011 [124]
	6.36	0.54	24.1 ^{a)}	51	Graphene/PbS/ZnO	-	2016 [125]
	5.4	0.56	18.2	53	MoO ₃ -Au-MoO ₃ /PbS/TiO ₂	9 days	2016 [126]

	9.01	0.55	24.8	66	MoO ₃ /PbS-TBAI, PbS-PDT/WPF-6-oxy-F/ZnO	-	2016 [127]
	8.3	0.62	21.5	62	PbS-MPA/PbS-PbI ₂ /CdS/ITO	-	2017 [87]
	9.3	0.65	25.3	65	PbS-ETD/PbS-TBAI/ZnMgO/ZnO	-	2017 [17]
	9.95	0.59 ^{a)}	25.4 ^{a)}	65.9	PbS-EDT:CuI/PbS-TBAI/carbon QDs/ZnO	-	2017 [128]
	6.47	0.54	24.2	49.5 ^{a)}	PbS/sputtered ZnO	>5 months	2017 [129]
	9.37	0.57	25.6	64	PbS-ETD/PbS-TBAI/SnO ₂ -Cl	-	2017 [116]
	9.7	0.62	23.8	66	PbS-ETD/PbS-TBAI/ordered wrinkled-ZnMgO	95 days	2017 [19]
	10.4	0.62	24.7	68	PbS-ETD/PbS-TBAI/ZnMgO	-	2017 [86]
HTL	3.5	0.58	15.6	35	MoO ₃ /PbS/ZnO	-	2011 [130]
	6.03	-	-	-	PbS QD/Ag nanocubes/ZnO NWs bulk heterojunction	-	2015 [131]
	10.6	0.65	22.8 ^{a)}	72.1 ^{a)}	Graphdiyne/PbS-ETD/PbS-TBAI/ZnO	120 days	2016 [132]
	9.60	0.57	27.9 ^{a)}	60	MoO ₃ /PTB7/i-CQDs/ZnO	141 day	2018 [18]
Others	1.68	0.24	14.0	50	PbS/PCBM	-	2010 [13]
	3.5	0.55	13.0 ^{a)}	49	Mesoscopic PbS/TiO ₂ NC/FTO	-	2012 [133]
	5.2	0.46	19.3	58	LiF/PbS	-	2013 [134]
	5.72	0.49 ^{a)}	25.3	46.6	MoO ₃ /PbS/PbS:CdSe/TiO ₂	-	2014 [135]
	4.2	1.06	8.3	48	1 eV PbS/RGL/1.6 eV PbS/TiO ₂	-	2015 [124]
	3.36	0.56	12.1	46.9	P3HT/PbS/ZnO	-	2015 [136]
	8.9	1.13	12.3	64.1	PbS-EDT/PbS-TABI/ZnO NC/Au/PbS-EDT/PbS-TBAI/ZnO	2 month	2017 [37]
	7.24	0.45	33.6	48	PbS/TiO ₂	>3600 h	2017 [83]
	10.5 ^{a)}	0.62	26.8	63.9	PbS-EDT/PbS-MAPbI ₃ +TG/ZnO	-	2017 [137]
	7.9	0.41	33.8	57	PbS-EDT/PbS-ZnI ₂ /MPA/AZO	70 days	2018 [138]
	9.9	0.64	24.6	63	PbS-EDT/PbS-PbX ₂ /AZO/Ag NWs	35 days	2018 [139]

^{a)} Here only the first three effective numbers are considered.

In order to engineer CTLs, charge transport layers (CTLs) using different materials (ZnO, SnO₂ and TiO₂) with doping and shape engineering (ZnO nanowires,[27, 90, 140] and SnO₂:Sb nanocrystals[141]) have been studied for reducing the interface

defect recombination in addition to exploration of new materials, e.g., graphene and silver nanowires, [139] which could have good electrical contact with the PbS CQD photoactive layer.[142, 143] From experiments, a larger number of defect states was observed within the bandgap of the PbS CQDs, which facilitates recombinations at the hetero-interfaces. Reducing the carrier concentration of the CTLs reduced this recombination.[21] An interfacial layer of ZnO with Mg doping ($\text{Zn}_{0.9}\text{Mg}_{0.1}\text{O}$) was demonstrated to reduce interfacial charge recombination and improve solar efficiency through an increased photo-voltage in PbS CQD solar cells (**Figure 10a&b**). Also, from transient photo-voltage (TPV) measurements, recombination time of the carriers is shown to be reduced as a result of the $\text{Zn}_{0.9}\text{Mg}_{0.1}\text{O}$ additional layer in the PbS CQD solar cell.[17] Upon N doping of the ZnO, the V_{OC} and efficiency of the PbS CQD device was also improved by 50% as a result of a decrease of carrier concentration in the ZnO (**Figure 10c**). In PbS CQD PVs, highly ordered wrinkled combustion-processed $\text{Zn}_{0.9}\text{Mg}_{0.1}\text{O}$ thin films also increase the charge-carrier extraction from the PbS CQD solid and diminish the interfacial charge recombination, leading to an increase from 8.4% to 9.7% in the efficiency.[19] Using SnO_2 doped by Cl as the ETL for PbS CQD PVs resulted in extended transmittance in the ultra violet (UV) region and improved lifetimes. In order to clarify the relation between doping and carrier lifetime, transient photo-current (TPC) measurements combined with TPV decay studies showed that the introduction of chlorine atoms could passivate the interface in the low-temperature-processed SnO_2 film. The transport lifetime ($\tau_t = 2.7 \mu\text{s}$) was prolonged to $3.8 \mu\text{s}$, and at the same time the charge recombination lifetime was

prolonged from 60 μs to 140 μs in the Cl-doped SnO_2 device. This result agrees well with the alleviated charge recombination at the device interfaces and the high PCE performance in SnO_2 -Cl devices (9.37%). [116] Similarly in TiO_2 , through Zr doping, the CTL matched with the CB of the PbS CQD film, so that the charge separation at the PbS/ TiO_2 interface was improved, yielding a V_{OC} of 0.38 V and PCE of 5.6%. [144] Also, N-doped TiO_2 nanowires can alter the band alignment between rutile TiO_2 and fluorine doped tin oxide (FTO), so that electron transfer from TiO_2 to the FTO electrode is more efficient. [145] Hyun *et al.* investigated the charge transfer from PbS CQDs with different nanometer sizes to TiO_2 nanoparticles, where the PbS CQDs are coupled to TiO_2 nanoparticles and are suspended in tetrachloroethylene. They found that PbS CQDs with smaller diameters (below 4.3 nm) could reduce the energy barrier with TiO_2 and enable more efficient charge transfer to the charge transport layer TiO_2 , consistent with stronger fluorescence quenching and more rapid fluorescence decays. [146]

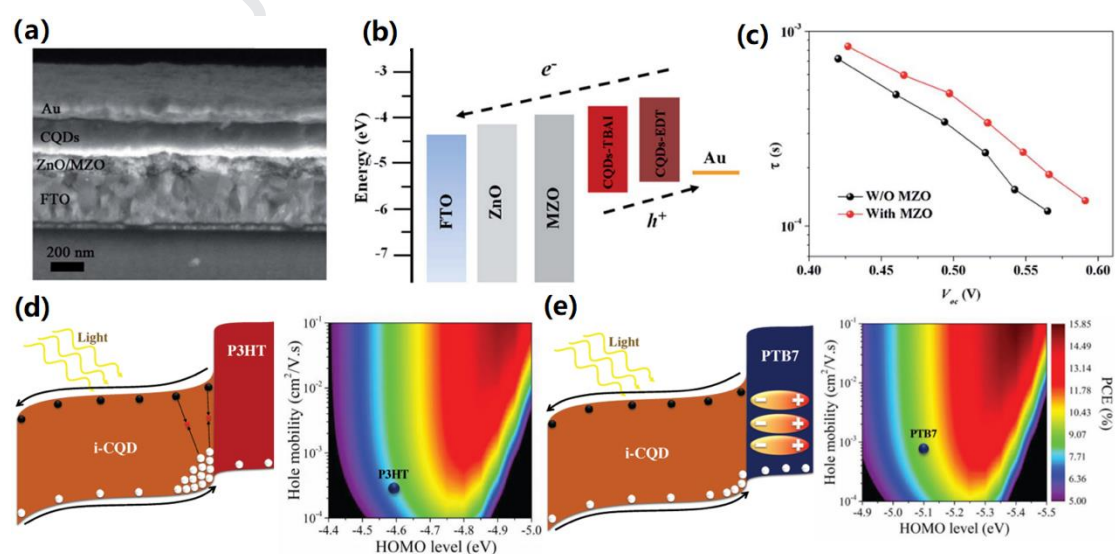


Figure 10. (a) Cross-sectional SEM image of PbS CQD PV with a $\text{Mg}_{0.9}\text{Zn}_{0.1}\text{O}$ buffer layer.

(b) Band diagram for the solar cell. (c) Carrier lifetime as a function of V_{OC} for the cells with/without the buffer layer. Reproduced with Permission.[17] Copyright 2017, Royal Chemical Society. Schematic illustration of charge accumulation and simulated device performance dependence on hole mobility and HOMO levels with HTL of (d) P3HT and (e) PTB7. Reproduced with Permission.[18] Copyright 2018, Wiley-VCH.

On the other hand, modification of the HTLs have also been shown to be useful in carrier transport, band alignment and improvement of PCE in PbS CQD PVs.[18, 130-132] In particular, the *n*-type oxide MoO_3 yielded a 4.4% efficiency, which represents a 65% improvement in comparison with the control device. The reason is that the HTL involves a dipole formation at the hetero-interface to enhance band bending and allow efficient hole extraction (**Figure 10d&e**).[147] Besides, Fermi level pinning can be avoided by using MoO_3 , through which the Schottky junction and impedance of extraction of holes from PbS can be prevented. In this way, the device performance was significantly enhanced, reflected by an improvement in efficiency related parameters and perhaps stability.[130]

Considering the limited mobility and high defect density in PbS CQDs, the charge collection rate can also be increased if the required diffusion length is reduced. Hence, it is necessary to increase the hetero-interface area,[66, 90, 140, 148] e.g., using nanowire structured electrodes to avoid a poor hole collection efficiency (**Figure 11a**).[149] Recently, nanostructured CTLs have been shown to be promising for highly efficient PbS CQD PVs.[149] In comparison with a planar structure, they have good penetration into the photo-active layer, so that the charge collection efficiency is improved due to an enlarged hetero-interface,[90] reduction in Fermi level pinning induced by charge recombination centers[150] and more sites for charge

separation.[151, 152] More importantly, architecture engineering using a so-called bulk nanoheterojunctions (BNH) using mixed PbS QDs with ZnO nanocrystals in conjunction with mixed ligand treatments were proved to passivate surface traps, which leads to a low V_{OC} deficit in PbS QDs of 0.4–0.55 V, compared with these (0.6–0.8) in conventional structure PbS CQD PVs.[153] In **Figure 11b–d**, the current is mapped to be more localized at the PbS-EDT/Au interface in the nanowire structure in comparison with the planar one.[68] This provides solid proof that the nanowire structure actually improves the charge extraction efficiency.

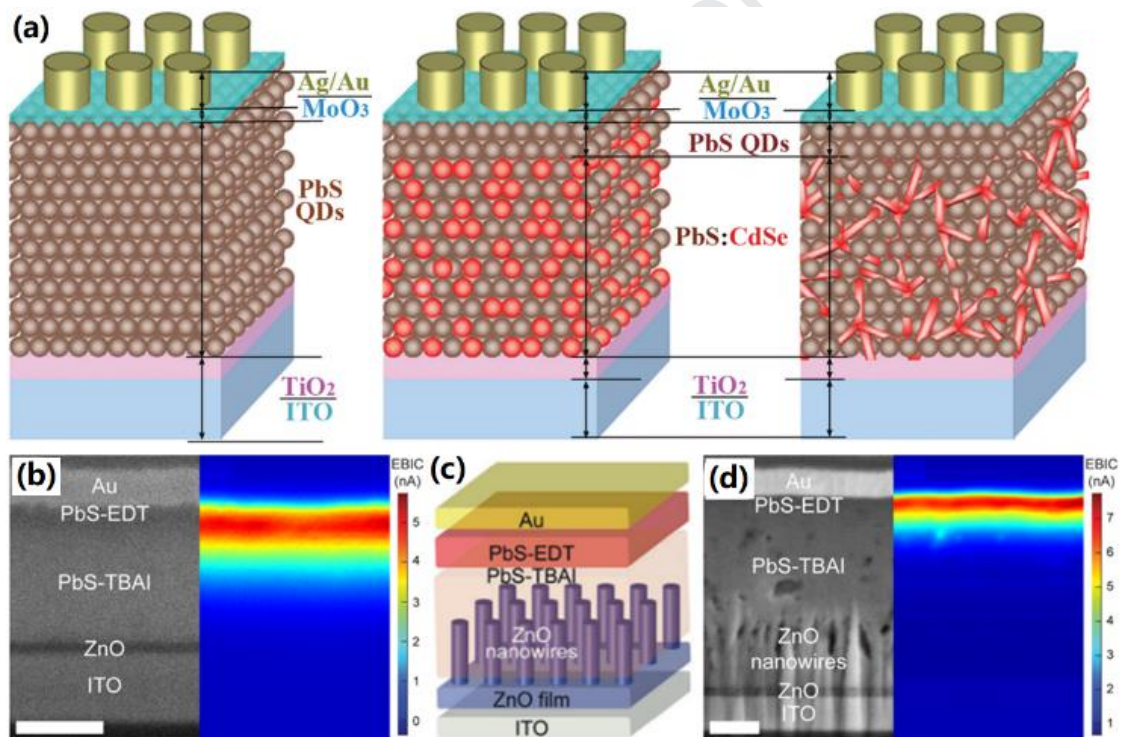


Figure 11. (a) Schematic drawings of the three type of solar cells: PbS CQD cell, b) PbS:CdSe CQD cell and c) PbS:CdSe nano-tetrapod cell. Reproduced with permission.[135] Copyright 2014, Wiley-VCH. (b) Cross-sectional SEM image and corresponding electron-beam-induced current maps for a planar PbS-TBAI/PbS-EDT solar cell. Reproduced with permission.[68] Copyright 2017, American Chemical Society. (c) Schematic of the device architecture that combines the ordered bulk heterojunction formed by the ZnO nanowire array for superior charge extraction. Reproduced with permission.[27] Copyright 2016, Wiley-VCH. (d) SEM/electron-beam-induced current images for a PbS-TBAI/PbS-EDT solar cell using a ZnO nanowire array to form an ordered bulk heterojunction. Reproduced with permission.[68] Copyright 2017, American

Chemical Society.

In addition, interface engineering through the use of novel electrodes (replacing ITO) and buffer layer are also demonstrated to be successful in achieving efficient charge extraction at the interface in addition to thermal treatment, leading to a leap in the PCE in the PbS CQD PVs. Zhang *et al.* studied the application of metallic silver nanowire network electrode as an alternative to ITO, due to their good light transmittance and high electrical conductivity in Ag nanowires. The PbS CQD PV shows a comparable experimental PCE of 9.7% using Ag nanowires with 10.8% in the device using an ITO layer. More importantly, PbS CQD PV using Ag nanowire electrodes maintains high-level photovoltaic performance under deformation and shows good durability after repeated cycles of compression and stretching, making them potentially suitable for applications in flexible PVs.[139] A CdI₂-treated CdSe CQD buffer layer has been introduced at the hetero-interface. Through optimization of the carrier concentration and energy band alignment by surface- and size-tunable electronic properties, the CdSe CQD buffer layer was also shown to suppress the interface recombination and to contribute additional photo-generated carriers, subsequently increasing both the V_{OC} and J_{SC} , leading to a 25% increase in PCE for the device.[154] Moreover, a thermal treatment is reported as a convenient way to improve V_{OC} with a reduction in interface defects.[30] At 140 °C, in particular, the device gives an optimized PCE value, reflected by an increase in J_{SC} rather than V_{OC} . However, further understanding of the effect of thermal annealing treatment on PbS

CQD PVs could lead to further enhancement of the stability issue.[155] Apart from the sol-gel process, devices using sputtered amorphous ZnO exhibit a particularly high J_{SC} together with PCE up to 6.47%. [95]

5 Challenges and Future Prospects for CQD PVs

Despite the significant progress made with defect passivation and engineering of CTLs, trap recombination still remains an important limiting factor for the efficiency of PbS CQD PVs, reflected by a large V_{OC} deficit (in Table 2&3). In addition, MEG solar cells using PbSe and PbTe exhibit lower PCE than conventional PbS CQD PVs. Therefore, we will focus on potential strategies that will overcome the aforementioned challenges.

Firstly, surface carrier recombination via the sub-bandgap defects are strongly correlated with the large V_{OC} deficit (0.6–0.8 V) in the PbS CQD PVs. Many surface modification strategies via ligand exchange as well as ‘soft methods’ have been applied to reduce this recombination without introducing new types of surface defects and is successful in improving the J_{SC} from 8.93–31.9 mA/cm². However, these strategies merely improve the V_{OC} s of the PbS CQD PVs. Thus, the role of surface defects and device architecture on non-radiative recombination at surfaces/interfaces should be further explored in order to gain further increases in PCEs in PbS CQD PVs.

In order to further passivate the sub-bandgap defects, it is necessary to further study the synthesis process of PbS CQD by the hot-inject method, so that the crystal

structure of the PbS CQDs are optimized with the {001} Pb terminating non-polar facet, so that undesirable hydroxyl ligands $[\text{OH}]^-$ are minimized during the synthesis of PbS CQDs. Also, the OA ligands should be avoided during PbS CQD growth by hot injection. At the same time, we expect that controlling the shape of PbS CQDs could provide another alternative route for achieve higher quantum efficiencies, as it was pointed that the QY of the PbSe NRs are enhanced than that for PbSe CQDs with a higher EQE (over 150%) was achieved in the PbSe NR PVs. Furthermore, new types of CQD materials other than PbS CQDs should also be explored for highly efficient PV applications. New types of nanocrystals with better transport properties should be explored for PVs. Among the newly emerged nanocrystals, $\alpha\text{-CsPbI}_3$ nanocrystals with defect tolerance have particularly attracted attention for the fabrication of highly efficient PV devices with prolonged stability of several months.[156, 157] Because they have shown a near-unity PLQY and high mobility ($0.2 \text{ cm}^2 \cdot \text{V}^{-1} \cdot \text{s}^{-1}$). In comparison with the $\alpha\text{-CsPbI}_3$ planar films, $\alpha\text{-CsPbI}_3$ nanocrystals also have demonstrated improved stability owing to their increased surface tension, so that the cubic $\alpha\text{-CsPbI}_3$ phase is sustained under 320°C , where the undesired orthorhombic phase can be induced. Currently, the experimental PCE for the $\alpha\text{-CsPbI}_3$ nanocrystals PVs can reach 14.32% with V_{OC} approaching the S-Q limit ($\sim 1.2 \text{ V}$).[158-163]

Secondly, in this study it has also been shown that interface defect passivation and band structure alignment via engineering of the charge transport layers, e.g., shape tuning and ionic doping as well as new electrode materials (silver nanowire,

graphene) have been explored and demonstrated to be successful in improving interface charge transport and charge carrier extraction in PbS CQD PVs. On the other hand, optical losses exist in the conventional transparent conductive oxides (TCOs). Light reflection and absorption by the front electrode are responsible for photon losses reaching ~30 % in the short wavelength region (400–600 nm), which is the wavelength range that is important for MEG.[126] From the TCO point of view, therefore, apart from the ETL engineering, it is beneficial for new materials with better balance between electrical conductivity and optical transmittance (e.g., SrVO_3 epi-layer grown using a molecular beam epitaxy at 850 °C [164]) could be incorporated as front electrodes in the PVs. Further investigations into wider bandgap ETLs in PbS and other types of CQD PVs would also be beneficial.

6 Conclusion

In summary, PbS CQDs are appealing for next generation solar cells with the possibility of efficiencies surpassing the S-Q limit through MEG. However, defect recombination limits the power conversion efficiencies and V_{OCs} . Through defect analysis, traps are located at 0.2–0.5 eV below the conduction band with a high-density of $\sim 10^{17} \text{ cm}^{-3}$, and are responsible for limiting the carrier lifetime and diffusion length. To passivate defects, different surface passivation strategies have been used to modify the surface chemistry, as well as the band structure to reduce the activity of interface defects. For further improvement, however, the surface stoichiometry of the CQDs should be studied so that the defect levels can be optimized. Also, it is

advantageous to explore the suitability of new types of CQDs with less defects and prolonged diffusion length for PVs. On the other hand, a nanowire ETL can be used to reduce the required diffusion length so that the carrier collection efficiency can be improved. For charge generation, it is also crucial to study the interference of the charge transport layer with the solar spectrum, so that the high energy photons are not filtered and can be used for multiple exciton generation. In order to do so, new types of UV transparent and highly conductive electrodes such as SrVO_3 are worth investigating.

Acknowledgments

The research funding from the China Postdoctoral Science Foundation through the project (No.:2018M640906) is greatly acknowledged by the authors. RLZH acknowledges funding from the Royal Academy of Engineering through the Research Fellowships scheme (No.: RF\201718\17101), the Isaac Newton Trust (Minute 19.07(d)) and Downing College Cambridge through the Kim and Juliana Silverman Research Fellowship. JLM-D acknowledges the Winton Programme for the Physics of Sustainability and funding from Bill Welland. Y.L. acknowledges that fundings from National Science Foundation of Shaanxi Province (no. 2019JQ-286) and the Scientific Research Program of Shaanxi Education Department (no.19JK0660). L.Q. was supported by the National Natural Science Foundation of China (Grant No.: 11774044).

Received: ((will be filled in by the editorial staff))

Revised: ((will be filled in by the editorial staff))

Published online: ((will be filled in by the editorial staff))

Conflict of Interest

The authors declare no conflict of interest.

References

- [1] Photovoltaics Report. <https://www.ise.fraunhofer.de/content/dam/ise/de/documents/publications/studies/Photovoltaics-Report.pdf> (accessed 01 June 2019).
- [2] K.-T. Kuo, D.-M. Liu, S.-Y. Chen, C.-C. Lin, *J. Mater. Chem.*, 19 (2009) 6780-6788.
- [3] J. Jean, P.R. Brown, R.L. Jaffe, T. Buonassisi, V. Bulović, *Energy Environ. Sci.*, 8 (2015) 1200-1219.
- [4] J. Jean, J. Xiao, R. Nick, N. Moody, M. Nasilowski, M. Bawendi, V. Bulović, *Energy Environ. Sci.*, 11 (2018) 2295-2305.
- [5] A.J. Nozik, *Physica E*, 14 (2002) 115-120.
- [6] M.C. Beard, J.M. Luther, O.E. Semonin, A.J. Nozik, *Acc. Chem. Res.*, 46 (2012) 1252-1260.
- [7] M.C. Hanna, A.J. Nozik, *J. Appl. Phys.*, 100 (2006) 074510.
- [8] V. Klimov, *Appl. Phys. Lett.*, 89 (2006) 123118.
- [9] G.H. Carey, L. Levina, R. Comin, O. Voznyy, E.H. Sargent, *Adv. Mater.*, 27 (2015) 3325-3330.
- [10] Y. Shang, Z. Ning, *Natl. Sci. Rev.*, 4 (2017) 170-183.
- [11] C. Murray, D.J. Norris, M.G. Bawendi, *J. Am. Chem. Soc.*, 115 (1993) 8706-8715.
- [12] M.A. Hines, G.D. Scholes, *Adv. Mater.*, 15 (2003) 1844-1849.
- [13] N. Zhao, T.P. Osedach, L.-Y. Chang, S.M. Geyer, D. Wanger, M.T. Binda, A.C. Arango, M.G. Bawendi, V. Bulovic, *ACS Nano*, 4 (2010) 3743-3752.
- [14] J.M. Luther, J. Gao, M.T. Lloyd, O.E. Semonin, M.C. Beard, A.J. Nozik, *Adv. Mater.*, 22 (2010) 3704-3707.
- [15] K. Szendrei, W. Gomulya, M. Yarema, W. Heiss, M.A. Loi, *Appl. Phys. Lett.*, 97 (2010) 203501.
- [16] J.E. Murphy, M.C. Beard, A.G. Norman, S.P. Ahrenkiel, J.C. Johnson, P. Yu, O.I. Mićić, R.J. Ellingson, A.J. Nozik, *J. Am. Chem. Soc.*, 128 (2006) 3241-3247.
- [17] X. Zhang, E.M.J. Johansson, *J. Mater. Chem. A*, 5 (2017) 303-310.
- [18] H. Aqoma, M.A. Mubarak, W. Lee, W.T. Hadmojo, C. Park, T.K. Ahn, D.Y. Ryu, S.Y. Jang, *Adv. Energy Mater.*, 8 (2018) 1800572.
- [19] X. Zhang, K. Welch, L. Tian, M.B. Johansson, L. Häggman, J. Liu, E.M.J. Johansson, *J. Mater. Chem. C*, 5 (2017) 11111-11120.
- [20] R.L. Hoyer, B. Ehrler, M.L. Böhm, D. Muñoz-Rojas, R.M. Altamimi, A.Y. Alyamani, Y. Vaynzof, A. Sadhanala, G. Ercolano, N.C. Greenham, *Adv. Energy Mater.*, 4 (2014) 1301544.
- [21] B. Ehrler, K.P. Musselman, M.L. Böhm, F.S. Morgenstern, Y. Vaynzof, B.J. Walker, J.L. MacManus-Driscoll, N.C. Greenham, *ACS Nano*, 7 (2013) 4210-4220.
- [22] C.-H.M. Chuang, A. Maurano, R.E. Brandt, G.W. Hwang, J. Jean, T. Buonassisi,

- V. Bulović, M.G. Bawendi, *Nano Lett.*, 15 (2015) 3286-3294.
- [23] A.J. Nozik, M.C. Beard, J.M. Luther, M. Law, R.J. Ellingson, J.C. Johnson, *Chem. Rev.*, 110 (2010) 6873-6890.
- [24] J. Tang, K.W. Kemp, S. Hoogland, K.S. Jeong, H. Liu, L. Levina, M. Furukawa, X. Wang, R. Debnath, D. Cha, K.W. Chou, A. Fischer, A. Amassian, J.B. Asbury, E.H. Sargent, *Nat. Mater.*, 10 (2011) 765.
- [25] A.H. Ip, S.M. Thon, S. Hoogland, O. Voznyy, D. Zhitomirsky, R. Debnath, L. Levina, L.R. Rollny, G.H. Carey, A. Fischer, *Nat. Nanotechnol.*, 7 (2012) 577.
- [26] C.-H.M. Chuang, P.R. Brown, V. Bulović, M.G. Bawendi, *Nat. Mater.*, 13 (2014) 796.
- [27] P.H. Rekemeyer, S. Chang, C.H.M. Chuang, G.W. Hwang, M.G. Bawendi, S. Gradečak, *Adv. Energy Mater.*, 6 (2016) 1600848.
- [28] X. Yao, Z. Song, L. Mi, G. Li, X. Wang, X. Wang, Y. Jiang, *Sol. Energy Mater. Sol. Cells*, 164 (2017) 122-127.
- [29] J.H. Song, H. Choi, Y.H. Kim, S. Jeong, *Adv. Energy Mater.*, 7 (2017) 1700301.
- [30] H. Aqoma, M. Al Mubarak, W.T. Hadmojo, E.H. Lee, T.W. Kim, T.K. Ahn, S.H. Oh, S.Y. Jang, *Adv. Mater.*, 29 (2017) 1605756.
- [31] R. Azmi, S. Sinaga, H. Aqoma, G. Seo, T.K. Ahn, M. Park, S.-Y. Ju, J.-W. Lee, T.-W. Kim, S.-H. Oh, *Nano Energy*, 39 (2017) 86-94.
- [32] K. Lu, Y. Wang, Z. Liu, L. Han, G. Shi, H. Fang, J. Chen, X. Ye, S. Chen, F. Yang, *Adv. Mater.*, 30 (2018) 1707572.
- [33] Y. Wang, K. Lu, L. Han, Z. Liu, G. Shi, H. Fang, S. Chen, T. Wu, F. Yang, M. Gu, *Adv. Mater.*, 30 (2018) 1704871.
- [34] M. Liu, Y. Chen, C.-S. Tan, R. Quintero-Bermudez, A.H. Proppe, R. Munir, H. Tan, O. Voznyy, B. Scheffel, G. Walters, A.P.T. Kam, B. Sun, M.-J. Choi, S. Hoogland, A. Amassian, S.O. Kelley, F.P.G.d. Arquer, E.H. Sargent, *Nat.*, 570 (2019) 96-101.
- [35] M.-J. Choi, F.P.G. de Arquer, A.H. Proppe, A. Seifitokaldani, J. Choi, J. Kim, S.-W. Baek, M. Liu, B. Sun, M. Biondi, B. Scheffel, G. Walters, D.-H. Nam, J.W. Jo, O. Ouellette, O. Voznyy, S. Hoogland, S.O. Kelley, Y.S. Jung, E.H. Sargent, *Nat Commun*, 11 (2020) 1-9.
- [36] B. Sun, A. Johnston, C. Xu, M. Wei, Z. Huang, Z. Jiang, H. Zhou, Y. Gao, Y. Dong, O. Ouellette, X. Zheng, J. Liu, M.-J. Choi, Y. Gao, S.-W. Baek, F. Laquai, O.M. Bakr, D. Ban, O. Voznyy, F.P. García de Arquer, E.H. Sargent, *Joule*, 4 (2020) 1542-1556.
- [37] G. Shi, Y. Wang, Z. Liu, L. Han, J. Liu, Y. Wang, K. Lu, S. Chen, X. Ling, Y. Li, *Adv. Energy Mater.*, 7 (2017) 1602667.
- [38] D. Wang, J.K. Baral, H. Zhao, B.A. Gonfa, V.V. Truong, M.A. El Khakani, R. Izquierdo, D. Ma, *Adv. Funct. Mater.*, 21 (2011) 4010-4018.
- [39] Y. Wei, Z. Ren, A. Zhang, P. Mao, H. Li, X. Zhong, W. Li, S. Yang, J. Wang, *Adv. Funct. Mater.*, 28 (2018) 1706690.
- [40] G.H. Carey, A.L. Abdelhady, Z. Ning, S.M. Thon, O.M. Bakr, E.H. Sargent, *Chem. Rev.*, 115 (2015) 12732-12763.
- [41] J.W. Jo, Y. Kim, J. Choi, F.P.G. de Arquer, G. Walters, B. Sun, O. Ouellette, J. Kim, A.H. Proppe, R. Quintero- Bermudez, J. Fan, J. Xu, C.S. Tan, O. Voznyy, E.H. Sargent,

- Adv. Mater., 29 (2017) 1703627.
- [42] A. Luque, A. Martí, A.J. Nozik, MRS Bull., 32 (2007) 236-241.
- [43] M.A. Watzky, R.G. Finke, J. Am. Chem. Soc., 119 (1997) 10382-10400.
- [44] A.R. Kirmani, A.D. Sheikh, M.R. Niazi, M.A. Haque, M. Liu, F.P.G. de Arquer, J. Xu, B. Sun, O. Voznyy, N. Gasparini, Adv. Mater., 30 (2018) 1801661.
- [45] J.Y. Kim, O. Voznyy, D. Zhitomirsky, E.H. Sargent, Adv. Mater., 25 (2013) 4986-5010.
- [46] N.T. Thanh, N. Maclean, S. Mahiddine, Chem. Rev., 114 (2014) 7610-7630.
- [47] W. Ostwald, Zeitschrift für Physikalische Chemie, 34U (1900) 495-503.
- [48] I.M. Lifshitz, V.V. Slyozov, J. Phys. Chem. Solids, 19 (1961) 35-50.
- [49] C.D. Wagner, J. Phys. Chem. Lett., 65 (1961) 2276-2277.
- [50] H. Reiss, J. Chem. Phys., 19 (1951) 482-487.
- [51] C. Burda, X. Chen, R. Narayanan, M.A. El-Sayed, Chem. Rev., 105 (2005) 1025-1102.
- [52] C.R. Kagan, E. Lifshitz, E.H. Sargent, D.V. Talapin, Sci., 353 (2016) aac5523.
- [53] R.D. Schaller, M. Sykora, J.M. Pietryga, V.I. Klimov, Nano Lett., 6 (2006) 424-429.
- [54] K. Kemp, C. Wong, S. Hoogland, E.H. Sargent, Appl. Phys. Lett., 103 (2013) 211101.
- [55] D. Zhitomirsky, O. Voznyy, L. Levina, S. Hoogland, K.W. Kemp, A.H. Ip, S.M. Thon, E.H. Sargent, Nat. Commun., 5 (2014) 3803.
- [56] R.D. Schaller, M. Sykora, S. Jeong, V.I. Klimov, J. Phys. Chem. B, 110 (2006) 25332-25338.
- [57] W. Ahmad, J. He, Z. Liu, K. Xu, Z. Chen, X. Yang, D. Li, Y. Xia, J. Zhang, C. Chen, Adv. Mater., 31 (2019) 1900593.
- [58] J.B. Sambur, T. Novet, B.A. Parkinson, Sci., 330 (2010) 63-66.
- [59] Y. Yan, R.W. Crisp, J. Gu, B.D. Chernomordik, G.F. Pach, A.R. Marshall, J.A. Turner, M.C. Beard, Nat. Energy, 2 (2017) 17052.
- [60] O.E. Semonin, J.M. Luther, S. Choi, H.-Y. Chen, J. Gao, A.J. Nozik, M.C. Beard, Sci., 334 (2011) 1530-1533.
- [61] M.L. Böhm, T.C. Jellicoe, M. Tabachnyk, N.J. Davis, F. Wisnivesky-Rocca-Rivarola, C. Ducati, B. Ehrler, A.A. Bakulin, N.C. Greenham, Nano Lett., 15 (2015) 7987-7993.
- [62] N.J. Davis, M.L. Böhm, M. Tabachnyk, F. Wisnivesky-Rocca-Rivarola, T.C. Jellicoe, C. Ducati, B. Ehrler, N.C. Greenham, Nat. Commun., 6 (2015) 8259.
- [63] C.S. Sandeep, S. Ten Cate, J.M. Schins, T.J. Savenije, Y. Liu, M. Law, S. Kinge, A.J. Houtepen, L.D.A. Siebbeles, Nat. Commun., 4 (2013) 2360.
- [64] T. Nishihara, H. Tahara, M. Okano, M. Ono, Y. Kanemitsu, J. Phys. Chem. Lett., 6 (2015) 1327-1332.
- [65] H. Wang, Y. Wang, B. He, W. Li, M. Sulaman, J. Xu, S. Yang, Y. Tang, B. Zou, ACS Appl. Mater. Interfaces, 8 (2016) 18526-18533.
- [66] K.S. Leschkies, A.G. Jacobs, D.J. Norris, E.S. Aydil, Appl. Phys. Lett., 95 (2009) 193103.

- [67] D. Zhitomirsky, O. Voznyy, S. Hoogland, E.H. Sargent, *ACS Nano*, 7 (2013) 5282-5290.
- [68] P.H. Rekemeyer, C.-H.M. Chuang, M.G. Bawendi, S. Gradecak, *Nano Lett.*, 17 (2017) 6221-6227.
- [69] D.D. Wanger, R.E. Correa, E.A. Dauler, M.G. Bawendi, *Nano Lett.*, 13 (2013) 5907-5912.
- [70] D. Zhitomirsky, M. Furukawa, J. Tang, P. Stadler, S. Hoogland, O. Voznyy, H. Liu, E.H. Sargent, *Adv. Mater.*, 24 (2012) 6181-6185.
- [71] L. Hu, M. Liu, A. Mandelis, A. Melnikov, E.H. Sargent, *Prog. Photovoltaics*, 25 (2017) 1034-1050.
- [72] I.J. Kramer, E.H. Sargent, *ACS Nano*, 5 (2011) 8506-8514.
- [73] Y.-X. Wang, S.-R. Tseng, H.-F. Meng, K.-C. Lee, C.-H. Liu, S.-F. Horng, *Appl. Phys. Lett.*, 93 (2008) 133501.
- [74] J.-T. Shieh, C.-H. Liu, H.-F. Meng, S.-R. Tseng, Y.-C. Chao, S.-F. Horng, *J. Appl. Phys.*, 107 (2010) 084503.
- [75] J. Jean, T.S. Mahony, D. Bozyigit, M. Sponseller, J. Holovský, M.G. Bawendi, V. Bulović, *ACS Energy Lett.*, 2 (2017) 2616-2624.
- [76] S. We, J. Jin, K.-S. Lee, G.W. Hwang, D.-K. Hwang, J.-H. Lee, *J. Korean Phys. Soc.*, 75 (2019) 985-989.
- [77] X. Jiang, H. Li, Y. Shang, F. Wang, H. Chen, K. Xu, M. Yin, H. Liu, W. Zhou, Z. Ning, *Chem. Commun.*, 55 (2019) 9483-9486.
- [78] M.C. Beard, *J. Phys. Chem. Lett.*, 2 (2011) 1282-1288.
- [79] A.A. Bakulin, S. Neutzner, H.J. Bakker, L. Ottaviani, D. Barakel, Z. Chen, *ACS Nano*, 7 (2013) 8771-8779.
- [80] D. Bozyigit, M. Jakob, O. Yarema, V. Wood, *ACS Appl. Mater. Interfaces*, 5 (2013) 2915-2919.
- [81] D. Bozyigit, S. Volk, O. Yarema, V. Wood, *Nano Lett.*, 13 (2013) 5284-5288.
- [82] J. Du, Z. Du, J.-S. Hu, Z. Pan, Q. Shen, J. Sun, D. Long, H. Dong, L. Sun, X. Zhong, *J. Am. Chem. Soc.*, 138 (2016) 4201-4209.
- [83] C. Ding, Y. Zhang, F. Liu, N. Nakazawa, Q. Huang, S. Hayase, Y. Ogomi, T. Toyoda, R. Wang, Q. Shen, *ACS Appl. Mater. Interfaces*, 10 (2017) 26142-26152.
- [84] K. Kushnir, K. Chen, L. Zhou, B. Giri, R.L. Grimm, P.M. Rao, L.V. Titova, *J. Phys. Chem. C*, (2018).
- [85] R.L. Hoyer, B. Ehrler, M.L. Böhm, D. Muñoz- Rojas, R.M. Altamimi, A.Y. Alyamani, Y. Vaynzof, A. Sadhanala, G. Ercolano, N.C. Greenham, *Adv. Energy Mater.*, 4 (2014) 1301544.
- [86] X. Zhang, P.K. Santra, L. Tian, M.B. Johansson, H.k. Rensmo, E.M.J. Johansson, *ACS Nano*, 11 (2017) 8478-8487.
- [87] L. Hu, R.J. Patterson, Y. Hu, W. Chen, Z. Zhang, L. Yuan, Z. Chen, G.J. Conibeer, G. Wang, S. Huang, *Adv. Funct. Mater.*, 27 (2017) 1703687.
- [88] D.C. Neo, C. Cheng, S.D. Stranks, S.M. Fairclough, J.S. Kim, A.I. Kirkland, J.M. Smith, H.J. Snaith, H.E. Assender, A.A.R. Watt, *Chem. Mater.*, 26 (2014) 4004-4013.
- [89] K.S. Jeong, J. Tang, H. Liu, J. Kim, A.W. Schaefer, K. Kemp, L. Levina, X. Wang,

- S. Hoogland, R. Debnath, ACS Nano, 6 (2011) 89-99.
- [90] H. Wang, T. Kubo, J. Nakazaki, T. Kinoshita, H. Segawa, J. Phys. Chem. Lett., 4 (2013) 2455-2460.
- [91] I. Mora-Sero, G. Garcia-Belmonte, P.P. Boix, M.A. Vazquez, J. Bisquert, Energy Environ. Sci., 2 (2009) 678-686.
- [92] R.L. Hoyer, B. Ehrler, M.L. Böhm, D. Muñoz-Rojas, R.M. Altamimi, A.Y. Alyamani, Y. Vaynzof, A. Sadhanala, G. Ercolano, N.C. Greenham, Adv. Energy Mater., 4 (2014) 1301544.
- [93] L. Hu, Z. Zhang, R.J. Patterson, Y. Hu, W. Chen, C. Chen, D. Li, C. Hu, C. Ge, Z. Chen, Nano Energy, 46 (2018) 212-219.
- [94] G.W. Hwang, D. Kim, J.M. Cordero, M.W. Wilson, C.H.M. Chuang, J.C. Grossman, M.G. Bawendi, Adv. Mater., 27 (2015) 4481-4486.
- [95] Y. Cao, A. Stavrinadis, T. Lasanta, D. So, G. Konstantatos, Nat. Energy, 1 (2016) 16035.
- [96] D. Zherebetsky, Y. Zhang, M. Salmeron, L.-W. Wang, J. Phys. Chem. Lett., 6 (2015) 4711-4716.
- [97] M. Yuan, M. Liu, E.H. Sargent, Nat. Energy, 1 (2016) 16016.
- [98] M. Liu, O. Voznyy, R. Sabatini, F.P.G. de Arquer, R. Munir, A.H. Balawi, X. Lan, F. Fan, G. Walters, A.R. Kirmani, Nat. Mater., 16 (2017) 258.
- [99] D. Kim, D.-H. Kim, J.-H. Lee, J.C. Grossman, Phys. Rev. Lett., 110 (2013) 196802.
- [100] Y. Cho, B. Hou, J. Lim, S. Lee, S. Pak, J. Hong, P. Giraud, A.-R. Jang, Y.-W. Lee, J. Lee, ACS Energy Lett., 3 (2018) 1036-1043.
- [101] X. Lan, O. Voznyy, A. Kiani, F.P. García de Arquer, A.S. Abbas, G.H. Kim, M. Liu, Z. Yang, G. Walters, J. Xu, Adv. Mater., 28 (2016) 299-304.
- [102] A. Stavrinadis, S. Pradhan, P. Papagiorgis, G. Itskos, G. Konstantatos, ACS Energy Lett., 2 (2017) 739-744.
- [103] X. Lan, O. Voznyy, F.P. García de Arquer, M. Liu, J. Xu, A.H. Proppe, G. Walters, F. Fan, H. Tan, M. Liu, Z. Yang, S. Hoogland, E.H. Sargent, Nano Lett., 16 (2016) 4630-4634.
- [104] M.J. Speirs, D.M. Balazs, D.N. Dirin, M.V. Kovalenko, M.A. Loi, Appl. Phys. Lett., 110 (2017) 103904.
- [105] S. Chen, Y.j. Wang, Q. Liu, G. Shi, Z. Liu, K. Lu, L. Han, X. Ling, H. Zhang, S. Cheng, Adv. Energy Mater., 8 (2018) 1701194.
- [106] Z. Yang, A. Janmohamed, X. Lan, F.P. García de Arquer, O. Voznyy, E. Yassitepe, G.-H. Kim, Z. Ning, X. Gong, R. Comin, Nano Lett., 15 (2015) 7539-7543.
- [107] R. Wang, X. Wu, K. Xu, W. Zhou, Y. Shang, H. Tang, H. Chen, Z. Ning, Adv. Mater., 30 (2018) 1704882.
- [108] R. Wang, Y. Shang, P. Kanjanaboos, W. Zhou, Z. Ning, E.H. Sargent, Energy Environ. Sci., 9 (2016) 1130-1143.
- [109] P.C. Clark, D.C. Neo, R. Ahumada-Lazo, A.I. Williamson, I. Pis, S. Nappini, A.A. Watt, W.R. Flavell, Langmuir, 34 (2018) 8887-8897.
- [110] J. Gao, J.C. Johnson, ACS Nano, 6 (2012) 3292-3303.
- [111] K.W. Kemp, A.J. Labelle, S.M. Thon, A.H. Ip, I.J. Kramer, S. Hoogland, E.H.

- Sargent, *Adv. Energy Mater.*, 3 (2013) 917-922.
- [112] S. Pradhan, A. Stavrinadis, S. Gupta, G. Konstantatos, *ACS Appl. Mater. Interfaces*, 9 (2017) 27390-27395.
- [113] R.M. Hewlett, M.A. McLachlan, *Adv. Mater.*, 28 (2016) 3893-3921.
- [114] J. Choi, Y. Kim, J.W. Jo, J. Kim, B. Sun, G. Walters, F.P. García de Arquer, R. Quintero- Bermudez, Y. Li, C.S. Tan, *Adv. Mater.*, 29 (2017) 1702350.
- [115] F. Yang, Y. Xu, M. Gu, S. Zhou, Y. Wang, K. Lu, Z. Liu, X. Ling, Z. Zhu, J. Chen, *J. Mater. Chem. A*, 6 (2018) 17688-17697.
- [116] J. Khan, X. Yang, K. Qiao, H. Deng, J. Zhang, Z. Liu, W. Ahmad, J. Zhang, D. Li, H. Liu, *J. Mater. Chem. A*, 5 (2017) 17240-17247.
- [117] G.-H. Kim, F.P. García de Arquer, Y.J. Yoon, X. Lan, M. Liu, O. Voznyy, Z. Yang, F. Fan, A.H. Ip, P. Kanjanaboos, *Nano Lett.*, 15 (2015) 7691-7696.
- [118] R. Azmi, H. Aqoma, W.T. Hadmojo, J.M. Yun, S. Yoon, K. Kim, Y.R. Do, S.H. Oh, S.Y. Jang, *Adv. Energy Mater.*, 6 (2016) 1502146.
- [119] H. Li, S. Jiao, J. Ren, H. Li, S. Gao, J. Wang, D. Wang, Q. Yu, Y. Zhang, L. Li, *Phys. Chem. Chem. Phys.*, 18 (2016) 4144-4153.
- [120] X. Cao, C.M. Li, H. Bao, Q. Bao, H. Dong, *Chem. Mater.*, 19 (2007) 3773-3779.
- [121] F. Eisner, A. Seitkhan, Y. Han, D. Khim, E. Yengel, A.R. Kirmani, J. Xu, F.P. García de Arquer, E.H. Sargent, A. Amassian, *Solar RRL*, 2 (2018) 1800076.
- [122] Y.-C. Chen, C.-H. Lin, T.-F. Guo, T.-C. Wen, *ACS Appl. Mater. Interfaces*, 10 (2018) 26805-26811.
- [123] M.A. Mahmud, N.K. Elumalai, M.B. Upama, D. Wang, V.R. Gonçalves, M. Wright, C. Xu, F. Haque, A. Uddin, *J. Power Sources*, 383 (2018) 59-71.
- [124] X. Wang, G.I. Koleilat, A. Fischer, J. Tang, R. Debnath, L. Levina, E.H. Sargent, *ACS Appl. Mater. Interfaces*, 3 (2011) 3792-3795.
- [125] B.-S. Kim, D.C. Neo, B. Hou, J.B. Park, Y. Cho, N. Zhang, J. Hong, S. Pak, S. Lee, J.I. Sohn, *ACS Appl. Mater. Interfaces*, 8 (2016) 13902-13908.
- [126] X. Zhang, C. Häggglund, M.B. Johansson, K. Sveinbjörnsson, E.M.J. Johansson, *Adv. Funct. Mater.*, 26 (2016) 1921-1929.
- [127] R. Azmi, H. Aqoma, W.T. Hadmojo, J.M. Yun, S. Yoon, K. Kim, Y.R. Do, S.H. Oh, S.Y. Jang, *Adv. Energy Mater.*, 6 (2016) 1502146.
- [128] Z. Ren, Z. Kuang, L. Zhang, J. Sun, X. Yi, Z. Pan, X. Zhong, J. Hu, A. Xia, J. Wang, *Solar RRL*, 1 (2017) 1700176.
- [129] S. Zang, Y. Wang, M. Li, W. Su, H. Zhu, X. Zhang, Y. Liu, *Sol. Energy Mater. Sol. Cells*, 169 (2017) 264-269.
- [130] P.R. Brown, R.R. Lunt, N. Zhao, T.P. Osedach, D.D. Wanger, L.-Y. Chang, M.G. Bawendi, V. Bulovic, *Nano Lett.*, 11 (2011) 2955-2961.
- [131] T. Kawawaki, H. Wang, T. Kubo, K. Saito, J. Nakazaki, H. Segawa, T. Tatsuma, *ACS Nano*, 9 (2015) 4165-4172.
- [132] Z. Jin, M. Yuan, H. Li, H. Yang, Q. Zhou, H. Liu, X. Lan, M. Liu, J. Wang, E.H. Sargent, *Adv. Funct. Mater.*, 26 (2016) 5284-5289.
- [133] L. Etgar, T. Moehl, S. Gabriel, S.G. Hickey, A. Eychmüller, M. Gratzel, *ACS Nano*, 6 (2012) 3092-3099.

- [134] C. Piliago, L. Protesescu, S.Z. Bisri, M.V. Kovalenko, M.A. Loi, *Energy Environ. Sci.*, 6 (2013) 3054-3059.
- [135] F. Tan, S. Qu, Q. Jiang, J. Liu, Z. Wang, F. Li, G. Yue, S. Li, C. Chen, W. Zhang, *Adv. Energy Mater.*, 4 (2014) 1400512.
- [136] X. Zhang, J. Zhang, J. Liu, E.M.J. Johansson, *Nanoscale*, 7 (2015) 11520-11524.
- [137] Z. Yang, J.Z. Fan, A.H. Proppe, F.P.G. de Arquer, D. Rossouw, O. Voznyy, X. Lan, M. Liu, G. Walters, R. Quintero-Bermudez, *Nat. Commun.*, 8 (2017) 1325.
- [138] Y. Bi, S. Pradhan, S. Gupta, M.Z. Akgul, A. Stavrinadis, G. Konstantatos, *Adv. Mater.*, 30 (2018) 1704928.
- [139] X. Zhang, V.A. Öberg, J. Du, J. Liu, E.M.J. Johansson, *Energy Environ. Sci.*, 11 (2018) 354-364.
- [140] J. Jean, S. Chang, P.R. Brown, J.J. Cheng, P.H. Rekemeyer, M.G. Bawendi, S. Gradečak, V. Bulović, *Adv. Mater.*, 25 (2013) 2790-2796.
- [141] Y. Bai, Y. Fang, Y. Deng, Q. Wang, J. Zhao, X. Zheng, Y. Zhang, J. Huang, *ChemSusChem*, 9 (2016) 2686-2691.
- [142] M. Morales- Masis, S. De Wolf, R. Woods- Robinson, J.W. Ager, C. Ballif, *Adv. Electron. Mater.*, 3 (2017) 1600529.
- [143] H. Wang, S. Yang, Y. Wang, J. Xu, Y. Huang, W. Li, B. He, S. Muhammad, Y. Jiang, Y. Tang, *Org. Electron.*, 42 (2017) 309-315.
- [144] H. Liu, J. Tang, I.J. Kramer, R. Debnath, G.I. Koleilat, X. Wang, A. Fisher, R. Li, L. Brzozowski, L. Levina, E.H. Sargent, *Adv. Mater.*, 23 (2011) 3832-3837.
- [145] Q. Qiu, S. Li, J. Jiang, D. Wang, Y. Lin, T. Xie, *J. Phys. Chem. C*, 121 (2017) 21560-21570.
- [146] B.-R. Hyun, Y.-W. Zhong, A.C. Bartnik, L. Sun, H.D. Abruna, F.W. Wise, J.D. Goodreau, J.R. Matthews, T.M. Leslie, N.F. Borrelli, *ACS Nano*, 2 (2008) 2206-2212.
- [147] J. Gao, C.L. Perkins, J.M. Luther, M.C. Hanna, H.-Y. Chen, O.E. Semonin, A.J. Nozik, R.J. Ellingson, M.C. Beard, *Nano Lett.*, 11 (2011) 3263-3266.
- [148] X. Lan, J. Bai, S. Masala, S.M. Thon, Y. Ren, I.J. Kramer, S. Hoogland, A. Simchi, G.I. Koleilat, D. Paz- Soldan, *Adv. Mater.*, 25 (2013) 1769-1773.
- [149] J.J. Cheng, C.-H.M. Chuang, O. Hentz, P.H. Rekemeyer, M.G. Bawendi, S. Gradečak, *ACS Appl. Mater. Interfaces*, (2018).
- [150] I.J. Kramer, D. Zhitomirsky, J.D. Bass, P.M. Rice, T. Topuria, L. Krupp, S.M. Thon, A.H. Ip, R. Debnath, H.C. Kim, *Adv. Mater.*, 24 (2012) 2315-2319.
- [151] D.A.R. Barkhouse, R. Debnath, I.J. Kramer, D. Zhitomirsky, A.G. Pattantyus- Abraham, L. Levina, L. Etgar, M. Grätzel, E.H. Sargent, *Adv. Mater.*, 23 (2011) 3134-3138.
- [152] N. Hjerrild, University of Oxford 2013.
- [153] S. Pradhan, A. Stavrinadis, S. Gupta, S. Christodoulou, G. Konstantatos, *ACS Energy Lett.*, 2 (2017) 1444-1449.
- [154] T. Zhao, E.D. Goodwin, J. Guo, H. Wang, B.T. Diroll, C.B. Murray, C.R. Kagan, *ACS Nano*, 10 (2016) 9267-9273.
- [155] J. Kurpiers, D.M. Balazs, A. Paulke, S. Albrecht, I. Lange, L. Protesescu, M.V. Kovalenko, M.A. Loi, D. Neher, *Appl. Phys. Lett.*, 108 (2016) 103102.

- [156] J. Gan, J. He, R.L. Hoye, A. Mavlonov, F. Raziq, J.L. MacManus-Driscoll, X. Wu, S. Li, X. Zu, Y. Zhan, X. Zhang, L. Qiao, ACS Energy Lett., 4 (2019) 1308-1320.
- [157] M. Hao, Y. Bai, S. Zeiske, L. Ren, J. Liu, Y. Yuan, N. Zarrabi, N. Cheng, M. Ghasemi, P. Chen, M. Lyu, D. He, J.-H. Yun, Y. Du, Y. Wang, S. Ding, A. Armin, P. Meredith, G. Liu, H.-M. Cheng, L. Wang, Nat. Energy, 5 (2020) 79-88.
- [158] A. Swarnkar, A.R. Marshall, E.M. Sanehira, B.D. Chernomordik, D.T. Moore, J.A. Christians, T. Chakrabarti, J.M. Luther, Science, 354 (2016) 92-95.
- [159] Q. Wang, Z. Jin, D. Chen, D. Bai, H. Bian, J. Sun, G. Zhu, G. Wang, S. Liu, Adv. Energy Mater., (2018) 1800007.
- [160] D. Ghosh, M.Y. Ali, D.K. Chaudhary, S. Bhattacharyya, Sol. Energy Mater. Sol. Cells, 185 (2018) 28-35.
- [161] J. Yuan, X. Ling, D. Yang, F. Li, S. Zhou, J. Shi, Y. Qian, J. Hu, Y. Sun, Y. Yang, Joule, 2 (2018) 2450-2463.
- [162] F. Liu, C. Ding, Y. Zhang, T. Kamisaka, Q. Zhao, J.M. Luther, T. Toyoda, S. Hayase, T. Minemoto, K. Yoshino, Chem. Mater., 31 (2019) 798-807.
- [163] K. Chen, W. Jin, Y. Zhang, T. Yang, P. Reiss, Q. Zhong, U. Bach, Q. Li, Y. Wang, H. Zhang, Q. Bao, Y. Liu, J. Am. Chem. Soc. 142 (2020) 3775-3783.
- [164] L. Zhang, Y. Zhou, L. Guo, W. Zhao, A. Barnes, H.-T. Zhang, C. Eaton, Y. Zheng, M. Brahlek, H.F. Haneef, Nat. Mater., 15 (2016) 204.

The authors declare no competing financial interest.

Journal Pre-proof

Declaration of interests

☒ The authors declare that they have no known competing financial interests or personal relationships that could have appeared to influence the work reported in this paper.

☐ The authors declare the following financial interests/personal relationships which may be considered as potential competing interests: